PRELIMINARY COPY

SUPPLEMENTAL SELECTED STUDIES OF VHF/UHF COMMUNICATIONS FOR PLANETARY (MARS/VENUS) RELAY LINKS

FINAL REPORT

CONTRACT NO. NAS2-3772

Prepared for

NATIONAL AERONAUTICS AND SPACE ADMINISTRATION
AMES RESEARCH CENTER
MOFFETT FIELD, CALIFORNIA

Prepared by

ASTRO-ELECTRONICS DIVISION
DEFENSE ELECTRONIC PRODUCTS
RADIO CORPORATION OF AMERICA
PRINCETON, NEW JERSEY

AED R-3210

Issued: September 18, 1967

PRELIMINARY COPY

PREFACE

This is the final report on "Supplemental Selected Studies of VHF/UHF Communications for Planetary (Mars, Venus) Relay Links", prepared by the Astro-Electronics Division of the Radio Corporation of America for the Ames Research Center, National Aeronautics and Space Administration under Contract No. NAS2-3772. The report covers work accomplished during the period from March 17 to September 30, 1967. All of the information presented here was initially highlighted in monthly reports and discussed in detail at the final oral report presented at the Ames Research Center in August 1967. Copies of the presentation material used in the oral report have been delivered to the Ames Research Center.

The major contributors to this report are Dr. H. Staras, Mr. S. H. Koth, Mr. W. Bisignani, and Mr. H. G. Rouland. Dr. Staras performed the multipath analysis for an exponential-type surface model (Task IA), and Mr. S. H. Roth and Mr. W. Bisignani were responsible for the performance of the fast-fading experimental investigation of a wideband non-coherent FSK system (Tasks 3, 4, and 6). Mr. Rouland provided the program technical management.

TABLE OF CONTENTS

TABLE OF CONTENTS (Continued)

LIST OF ILLUSTRATIONS

LIST OF ILLUSTRATIONS (Continued)

SECTION I

INTRODUCTION AND SUMMARY

A. INTRODUCTION

1. Background

The specific studies performed by **RCA** during this program supplemented and extended available analytical information relative to communications problems between a probe entering a planetary atmosphere and **a** nearby spacecraft bus, based on two probe trajectories representative of entry from a flyby mission and from an orbit mission. The study comprised four **tasks:**

- Investigation of multipath environment using an exponential surface model of Mars and Venus;
- Experimental determination of the effects of fast fading on the wideband noncoherent FSK relay link with hardwire bit synchronization;
- Experimental determination of the effects of fast fading on the relay-link receiver with bit synchronization; and
- Experimental determination of fast fading on the distribution of errors as a function of the mission profile.

The original multipath analysis performed under this contract was based on an analytic surface model (two-dimensional Gaussian distribution) and led to useful results in defining the multipath environment (average scattered power and fading

bandwidth from an extended surface). Radar data from the moon and other planets indicates that the planet surface may be slightly rougher or more diffuse than the analytic surface model implies. At the beginning of the study, it was felt that a non-analytic surface with an exponential correlation function would be a more representative surface model than the analytic surface model.

The purpose of Task 1A, "Multipath Propagation Study," was to refine the multipath analysis by utilizing the non-analytic surface. The scattering function for an extended surface could not be solved in closed form but was solved using a numerical procedure. The scattering formula derived for an extended rough surface with an exponential correlation function yielded results of such doubtful accuracy as to make the validity of the approach highly suspect. Analysis of the basic formulation showed the conservation of incident power to aggregate of the reflected power is not satisfied for differential areas with unity reflection coefficients. Attempts to "doctor" the formulation were not successful.

The basic analysis of the scattered power from an extended exponential surface is presented in Section If, "Multipath Propagation Study (Task 1A). "Additional discussion of this analysis, including recommendations, is presented in Section I, Paragraph B, "Special Notes on Multipath Propagation Study (Task 1A)."

The previous study considered the effects of slow fading, which is the worst case, on the performance of a wideband noncoherent FSK link. For the low data rates of interest (100 to 300 bits per second), the multipath analysis showed that

the link would be operating in a fast-fading environment. In order to experimentally determine the effects of fast fading, a simulator was assembled with three discrete fading bandwidths, continuously variable γ^2, and doppler offset of the reflected signal with respect to the direct signal. The simulator discription and the effects of fast fading on the wideband noncoherent FSK system are discussed in Task 3, "Experimental Investigation of Fast Fading." The effects of fast fading on bit synchronization is discussed in Task 4.

In the case of slow fading, the fading period is long compared to a data bit. When the link is in a fade, many bits are affected and the errors are not independent. Therefore, the mean probability of error may not be as meaningful as the percentile probability of error, which was discussed in the previous study. The purpose of Task 6, "Link Performance Criteria" is to experimentally determine the effects of moderately fast fading on the distribution of errors as a function of fading environment corresponding to three different points in the probe after entry into the atmosphere (near end of blackout, midway to impact, and near terminal impact). This is especially important since the aggregate of all the data transmitted from the probe may not be sufficient for a good statistical sample.

2. Summary of Task Description and Results

The study comprised analysis of multipath propagation for a non-analytic planetary surface model and experimental investigation to determine the effects of fast fading, which is expected for a probe entry mission, on the communication link. A summary of results for the multipath progagation task is presented in Paragraph B of this section,

The experiments utilized the breadboard system developed earlier under this contract. Unless otherwise specified, the receiver was operated at a data rate of 100 bits per second which corresponds to a WT of 100. As part of the experimental effort, a fast fade generator was developed with the following characteristics:

Fading Bandwidth	**200 Hz, 1000 Hz** and **3000 Hz**
γ^2 (variable)	0 to ∞
Doppler Offset	**0 Hz** to **10,000 Hz**

For the above fading bandwidths and a data rate of 100 bits per second, the fading rates (BT) are 2, 10, and **30.**

The results of the experimental determination of fast-fading environment on a wideband noncoherent FSK system are:

- The effect of increasing fading bandwidth (for a constant reflected power) is to improve the link performance. The performance can be superior to the no-multipath case, but improvement beyond the no-multipath case cannot be utilized in the mission since it relies on the presence of the reflected signal, which can only be postulated, but not guaranteed.
- The effect of increasing differential doppler offset (for a constant reflected power) is to improve link performance.
- The bit synchronizer introduces approximately 0.5 db to 1.0 db degradation in link performance in a nonfading environment. While

previous tests indicated that slow fading adversely affected the performance of the bit synchronizer, the results here show that fast fading does not measurably degrade the performance of the bit synchronizer.

- Fast fading ($BT \geq 2$) does not cause any measurable clustering of errors. Since the errors are essentially independent, the mean or average probability of error is a valid measure of link performance.
- The limit of improvement in link performance, due to fast fading, increasing doppler offset, or any combination of the two, is to consider the received signal energy as the sum of the direct and reflected energy.

B. SPECIAL NOTES ON THE MULTIPATH PROPAGATION STUDY

1. Background

In the previous study performed under this contract,' formulas were derived for the amplitude of the reflected signal relative to that of the transmitted (direct) signal, the polarization of the reflected signal, and the fading bandwidth of the reflected signal. The analysis was based on an analytic planetary surface model which was developed initially by Beckmann and Spizzichino' for differential surface areas. The original effort by RCA was to determine the amplitude and distribution of the reflected signal from an extended surface (based on the Beckmann and Spizzichino formulations), which would be illuminated by a probe or satellite near the planet's surface. The principal assumptions associated with this approsch are summarized below:

(1) The rough surface is Gaussian, with $\sigma/\lambda \gg 1$, where σ is the rms "bump" height, and λ is the radio wavelength.

(2) The rms slope of the surface is fairly small. Mathematically, this is written as $\sigma/T \ll 1$, where T is the correlation length of the surface undulations.

(3) The rough surface correlation function is analytic. The mathematical implications of this are discussed by Beckmann[3], as well as others,

(4) Shadowing of one part of the surface by another, as well as multiple scattering are not important considerations. This is a satisfactory approximation only as long as (2) and (3), above, are satisfied.

The generally accepted solution for the scattered signal from the analytic surface based on these assumptions is that the energy is concentrated in a narrow beam centered about the specular direction. Review of radar data from the moon, however, suggests that some of the energy should appear in sidelobes (implying a slightly rougher or more diffuse surface than is indicated by the analytic surface model), and that a non-analytic surface (specifically one with an exponential correlation function) would be more representative, More recently, another paper[4] appeared describing model studies of acoustic scattering from a rough surface which also suggested that the exponential correlation function provides a more reasonable fit to the experimental data than the analytic function.

The purpose of the study reported on here was to determine the significant multi-path parameters from an extended exponential surface to obtain the second order (sidelobe) effects associated with a surface which scatters somewhat more diffusely than one characterized by an analytic surface.

2. Summary of Results

For the analytic surface previously studied, the rough planetary surface was characterized by T/σ, which represents the reciprocal of the rms slope of the surface undulations. For the non-analytic surface postulated for this portion of the study, the rough surface was characterized by a parameter, p, which is proportional to $(T/\sigma)(\lambda/\sigma)$. While T/σ is large, λ/σ is small for a rough surface. The surface of Mars, Venus, and the moon are probably characterized by p's of the order of 1.

For the p's of interest, the scattering formula derived for an extended rough surface with an exponential correlation function yielded results of such doubtful accuracy as to make the validity of the approach highly suspect. Analysis of the basic formulation showed that for small values of p, the required conservation of incident power in the aggregate of the reflected power is not satisfied even for differential areas and unity reflection coefficients. Attempts to "doctor" the formulation were not successful, Only for values of p greater than 10 (which are not of interest in this study) did the scattering form-ula appear to approach validity. Inspection of the numerical computations indicate that the formulations attribute excessive scattering power near grazing angles.

The exponential correlation function was known at the outset of the study to be unrealistic[5], since the first derivative of the function is not zero at the origin (a necessary condition for complete validity). However, it was hoped that it would furnish information regarding reflection distributions away from the origin (sidelobes). In particular, the exponential correlation function implies that the slopes of the surface undulations can be extremely high, and such high slopes explain why the resulting scattering function is highly diffuse. However, the existence of such slopes conflict with a basic assumption used in deriving the scattering function: namely, that the rms slope is small. Furthermore, the steep slopes imply that significant shadowing and multiple scattering occur, which also conflicts with an explicit assumption used in deriving the scattering function (see Paragraph 1, above).

It is of interest to note that the analytic surface model studied previously does satisfy conservation of power requirements. It is felt that a modification of the generally accepted solution for the reflected signal from an analytic surface will yield better estimates for the scattering pattern away from the specular direction.

3. Recommendations

The two-part analytic study performed under this contract has highlighted a topic in this subject of radio-wave scattering from a rough surface which deserves further elucidation.

The analytic correlation function assumed in the first part of the study gave rise to a scattering function which was highly concentrated around the specular direction

and decayed very rapidly away from the main lobe. This decay was more rapid than experimental data seem to suggest. To accommodate the experimentally observed slower decay, various investigators have suggested the use of an exponential correlation function (which is, of course, not analytic at the origin). While the exponential correlation function does indeed give rise to a scattering function which decays more slowly away from the main lobe, the present study has demonstrated that it has another serious flaw; namely, it does not satisfy the conservation of power requirement. Specifically, what is meant by this is: the scattering function that results from the use of the exponential correlation is of such a mathematical form that the total power (i.e., over all directions) scattered from an element of surface is not equal to the incident power intercepted by the element of surface. This failure to satisfy the conservation of power requirement implies that its use in calculating the average scattered power from an extended surface is of doubtful validity. It, therefore, appears desirable to find a more satisfactory analytic formulation of the problem. The following mathematical considerations suggest that this may be possible.

Beckmann and Spizzichino have shown that the scattering function, P_s, can be written

$$P_s \approx F^2 \int \tau J_o (v_{xy} \tau) e^{-g[1-C(\tau)]} d\tau \qquad \text{(I-1)}$$

where

$$F = \frac{1 + \cos\theta_1 \cos\theta_2 - \sin\theta_1 \sin\theta_2 \cos y}{\cos\theta_1 + \cos\theta_2}$$

$$v_{xy}^2 = k^2 (\sin^2\theta_1 + \sin^2\theta_2 - 2 \sin e_1 \sin e_2 \cos y)$$

$$g = k^2 \sigma^2 (\cos\theta_1 + \cos\theta_2)^2$$

$C(\tau)$ = surface correlation function

Since g is assumed to be very large, it has always been assumed that $C(\tau)$ need be known only in the neighborhood of $\tau = 0$ where $C \approx 1$. Therefore, one of two assumptions have been made in the past. Either $C(\tau) \approx 1 - \frac{\tau^2}{T^2}$, or $C(\tau) \approx \frac{\tau}{T}$, the first being the approximate form for an analytic correlation function, while the second is the appropriate approximation for the exponential correlation function. Upon further reflection, it appears that the analytic approximation mentioned above is probably valid when $g >> v_{xy}T$ (namely, not too far from the specular direction); however, it is probably not valid when $g << v_{xy}T$ (namely, quite far from the specular direction). It would appear that further study of the integral in Equation I-1, especially from the viewpoint of finding an asymptotic form for P_s when $g << v_{xy}T$ even if $C(\tau)$ is analytic, would help clarify the whole question of scattering from extended surfaces.

REFERENCES

1. "Selected Studies of VHF/UHF Communications for Planetary (Mars/Venus) Relay Links," RCA Final Report prepared for NASA, Ames. Res, Center, under Contract No. NAS 2-3772 (See, in particular, section describing Task V).

2. Beckmann, P. and A. Spizzichino, "The Scattering of Electromagnetic Waves from Rough Surfaces," Pergamon Press, McMillan Co., New York 1963.

3. Beckmann, P., "Scattering by composite rough surfaces," Proc. IEEE, Vol. 53, pp. 1012-1015, Aug. 1965.

4. Horton, C. W., et al, "Model studies on the scattering of acoustic waves from a rough surface," J. Acoust. Soc. Am., Vol. 41, pp. 635-643, April 1966.

5. Middleton, D., "An Introduction to Statistical Communication Theory," McGraw-Hill, New York, 1960.

SECTION II

MULTIPATH PROPAGATION STUDY (TASK 1A)

A. SUMMARY

This study considers the effects of a rough planetary surface on certain communications system parameters of interest that arise in various planetary exploration missions. The study represents an extension of an earlier study performed under this contract. It differs from the earlier one in that the correlation function that describes the surface roughness was assumed in the present study to be exponential rather than analytic,* The physical implication of this new assumption about the correlation function is that the pattern of incoherent scatter from the rough surface is more diffuse than it was under the assumption of the earlier study.

It was hoped to evaluate analytically the average scattered power and the fading rate. Unfortunately, this hope was not realized. The diffuse scattering function is so complicated that it was impossible to find a satisfactory analytic evaluation of the total scattered power, let alone the fading rate. It was decided, therefore, to put the integral for the average scattered power on a computer. This numerical computation procedure brought to light a basic defect in the formulation of

* The exponential correlation function is, of course, not analytic at the origin, since it is assumed that there is an exponential decay on both sides of the origin.

the problem, a defect that makes evaluation of the average scattered power from an extended surface somewhat suspect in the case of diffuse scattering, This will be discussed in some detail in the body of this section.

Since no analytical procedure was found that would permit closed-form evaluation of the average scattered power, it was not possible to carry out the other integrations that would have yielded the fading rate. However, the basic physical principle suggests that the fading rate in the case of very diffuse scattering would be higher than in the case of directional scattering, since the size of the effective scattering region is larger.

B. THE AVERAGE SCATTERED POWER

1. Analysis

a. Basic Formulation

In the previous study' (i.e., based on the assumption of an analytic correlation function), it was shown that the ratio of the average scattered power to the direct power can be written

$$\frac{\langle P_s \rangle}{P_d} = \int P_o \, dS \qquad \text{(II-1)}$$

$$P_o = \frac{|R|^2}{4\pi} \frac{\cot 4\beta_o}{r_1^2 r_2^2 \cos\beta} \exp\left(-\frac{\tan^2\beta}{\tan^2\beta_o}\right) \qquad \text{(II-2)}$$

where $\tan \beta_o = \frac{2\sigma}{T}$ ($\sim$ rms slope of surface undulations),

$$\tan^2\beta = \frac{\sin^2\theta_1 + \sin^2\theta_2 - 2\sin\theta_1 \sin\theta_2 \cos\varphi}{(\cos\theta_1 + \cos\theta_2)^2},$$

and R is the Fresnel reflection coefficient for a plan surface.

The various angles and distances defined above are the same as those defined in earlier study but are presented in Figure 11-I for convenience. In the present study (i.e., based on the assumption of an exponential correlation function), Equation (II-1) still applies, but Equation (II-2) must be rewritten to read

$$P_o = \frac{T^2}{2\pi k^2 \sigma^4} \frac{|R|^2 r^2}{r_1^2 r_2^2} \frac{\left[1+\cos\theta_1\cos\theta_2 - \sin\theta_1\sin\theta_2\cos\varphi\right]^2}{(\cos\theta_1+\cos\theta_2)^6 \left[1+\frac{T^2}{k^2\sigma^4} f^2\right]^{3/2}} \qquad \text{(II-3)}$$

where

$$f^2 = \frac{\sin^2\theta_1 + \sin^2\theta_2 - 2\sin\theta_1 \sin\theta_2 \cos\varphi}{(\cos\theta_1 + \cos e,)^4}$$

$$k = \frac{2\pi}{\lambda} = \frac{\omega}{c}$$

Equation (11-3) differs from Equation (11-2) in two important respects. First of all, Equation (II-2) is frequency independent, while Equation (II-3) is frequence dependent. Secondly, if $T/\sigma \gg 1$, Equation (II-2) decays more rapidly away from the specular point (where $\tan\beta = 0$) than does Equation (11-3). There are two reasons for the less rapid decay of Equation (II-3) compared to Equation (II-2). One is that the important parameter is not T/σ (which is very large) but rather $T/\sigma \div k\sigma$, where $k\sigma$ is also very large. It is possible that $\frac{T}{k\sigma^2}$ is not much larger

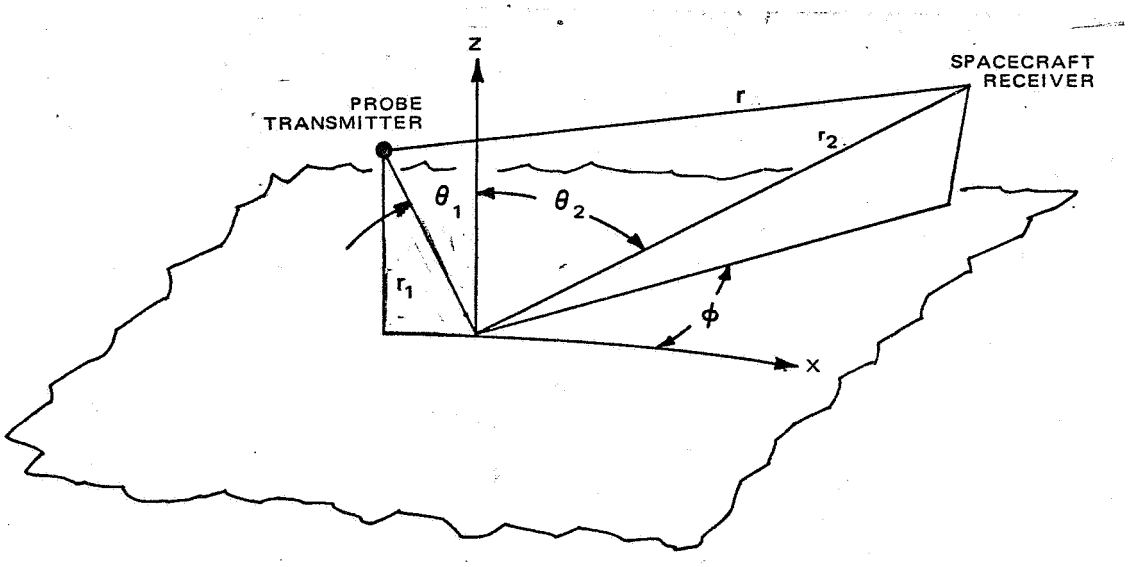

Figure II-1. Geometrical Parameters Associated with Scattering from a Rough Surface

than unity, and is perhaps substantially smaller. The other reason is the presence of an inverse 3/2 power decay from the specular point, which is of course a far slower decay than the exponential function in Equation (II-2).

After many attempts to find approximate analytic solutions for Equation (II-1) using Equation (11-3) as the integral, it was decided that none of these were sufficiently reliable. Not being able to evaluate Equation (II-I)analytically, it was decided to use numerical methods. Luckily, the integration over φ can be done in closed form to obtain a complicated sum of complete elliptic integrals. Minor manipulation of Equation (II-3) permits the representation

$$I = \frac{p^2}{R} \int_0^{\rho_o} \int_0^{\pi} \frac{|R|^2 \left[1+\cos(\theta_1-\theta_2 - 2\sin\theta_1 \sin e_2 \cos^2 \frac{\varphi}{2}\right]^2}{r^2 \left[(\cos\theta_1+\cos\theta_2)^4 + p2(\sin e_1+\sin\theta_2)^2 - 4p^2 \sin e_1 \sin e_2 \cos^2 \frac{\varphi}{2}\right]^{3/2}} \rho d\rho d\varphi \quad \text{(II-5)}$$

Substituting $\psi = \frac{\pi}{2} - \frac{\varphi}{2}$ yields

$$I = \frac{2p^2}{\pi} \int_0^{\rho_o} \frac{|R|^2 \rho d\rho}{r^2 \left[(\cos\theta_1+\cos\theta_2)^4 + p^2(\sin\theta_1+\sin\theta_2)^2\right]^{3/2}} \int_0^{\pi/2} \frac{N(\psi)}{D(\psi)} d\psi \quad \text{(II-6)}$$

where

$$N = \left[1+\cos(\theta_1-\theta_2)\right]^2 - 4\left[1+\cos(\theta_1-\theta_2)\right]\sin\theta_1 \sin\theta_2 \sin^2\psi + 4\sin^2\theta_1 \sin^2 e_2 \sin^4\psi$$

$$D = \left\{1 - \frac{4p2\sin\theta_1 \sin\theta 2}{(\cos\theta_1+\cos\theta_2)^4 + p^2(\sin\theta_1+\sin\theta_2)^2} \sin 2\psi\right\}^{3/2}$$

The integral over Ψ is now in the standard form of the elliptic integrals. Introducing $q^2 = (\cos\theta_1+\cos\theta_2)^4 + p^4 (\sin\theta_1+\sin\theta_2)^2$ and $k^2 = \frac{4p^2}{q^2} \sin\theta_1\sin\theta_2$, we obtain

$$n^2 \int_o \frac{|R|^2 \rho\, d\rho}{r^2 q^3} \left\{ \int_o^{\pi/2} \frac{\left[1+\cos(\theta_1-\theta_2)\right]^2}{(1-k^2\sin^2\psi)^{3/2}} d\psi - 4\sin\theta_1\sin\theta_2 \left[1+\cos(\theta_1-\theta_2)\right] \int_o^{\pi/2} \frac{\sin^2\psi}{(1-k^2\sin^2\psi)^{3/2}} d\psi \right.$$

$$\left. \ldots + 4\sin^2\theta_1\sin^2\theta_2 \int_o^{\pi/2} \frac{\sin^4\psi\, d\psi}{(1-k^2\sin^2\psi)^{3/2}} \right\}$$

$$2p^2 \int \frac{|R|^2 \rho\, d\rho}{r^2 q^3} \left\{ \frac{\left[1+\cos(\theta_1-\theta_2)\right]^2}{1-k^2} E(k^2) - 4\sin\theta_1\sin\theta \left[1+\cos(\theta_1-\theta_2)\right] \frac{E(k^2)-(1-k^2)K(k^2)}{k^2(1-k^2)} \right.$$

$$\left. + 4\sin^2\theta_1\sin^2\theta_2 \frac{(2-k^2)E(k^2)-2(1-k^2)\,K(k^2)}{(1-k^2)\,k^4} \right\} \qquad \text{(II-7)}$$

Equation (II-7) was evaluated numerically with the aid of the following transformation (refer to Figure 11-2):

$x = \cos\theta_1 = \frac{h}{r}$ $\qquad dx = -\sin\theta_1 d\theta_1$

$p = h\tan\theta_1$ $\qquad dp = \frac{h}{\cos^2\theta_1} d\theta_1$

$$\frac{p\,dp}{r^2} = -\frac{dx}{x}$$

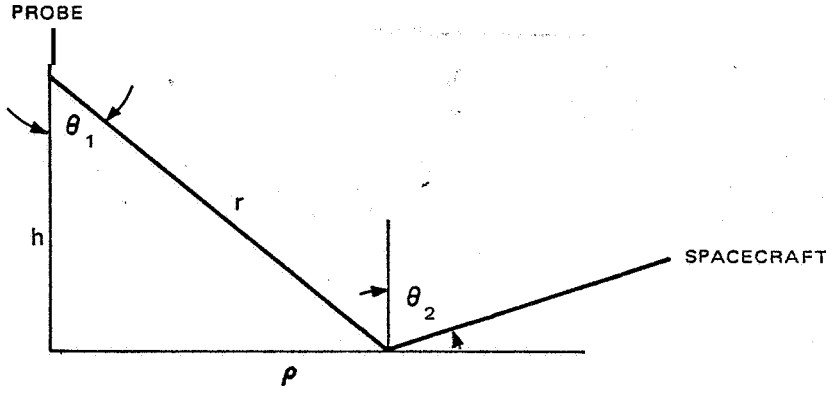

Figure **If-2.** Geometric Parameters Used to Effect Transformation from Equation **(II-7)** to Equation **(II-8)**

Thus, as programmed for the computer, the integral in question becomes

$$I = \frac{2p^2}{\pi} \int_{\epsilon}^{1} |R|^2 \frac{dx}{xq^3} \left\{ \frac{\left[1+xc+\sqrt{(1-x^2)(1-c^2)}\right]^2}{1-k^2} E(k^2) + \ldots \right.$$

$$\ldots -4\sqrt{(1-x^2)(1-c^2)} \left[1+xc+\sqrt{(1-x^2)(1-c^2)}\right] \frac{E(k^2)-(1-k^2)K(k^2)}{k^2(1-k^2)} + \ldots$$

$$\left. \ldots +4(1-x^2)(1-c^2) \frac{(2-k^2)E(k^2) - 2(1-k2)K(k2)}{k^4(1-k^2)} \right\} \qquad \text{(II-8)}$$

The parameters **q** and k were defined earlier, and $c = \cos \theta_2$. It should be explicitly noted that the x in the denominator of the integral in Equation (11-8) would make the integral diverge, if the lower limit would go to zero. As will be explained in the next few paragraphs, there is good physical reason to put a finite lower limit at ϵ. Unfortunately, however, the integral depends (by factors of 2 or 3) on just where the lower limit is placed.

b. The Lower Limit Question

Figure 11-3 indicates the maximum that θ_1 can be when considering the spherical character of the planetary surface. This largest value, θ_{1m}, satisfies the relation:

$$\sin\theta_{1m} = \frac{a}{a+h} \simeq 1 - \frac{h}{a} \qquad \text{(II-9)}$$

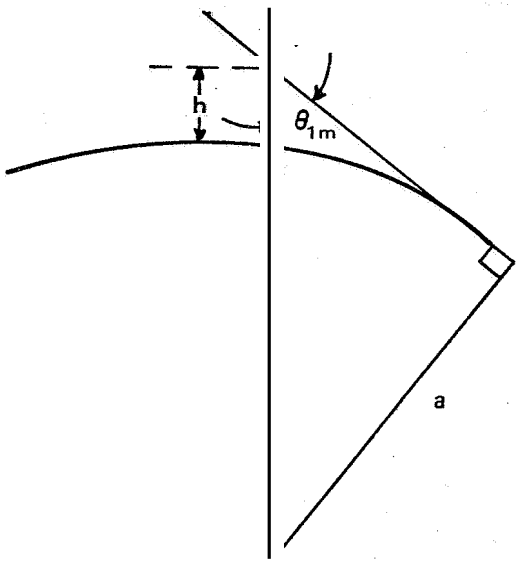

Figure **II-3.** Geometry for Estimating $E = \text{Cos } \theta_{1m}$

where h is the altitude of the planetary probe, and a is the radius of the planet. From Equation (11-9), it should be clear than $\sin\theta_{1m}$ is near unity and, therefore, $\epsilon = \cos\theta_{1m}$ is a very small quantity. From this, we can write:

$$\sin\theta_{1m} = \sqrt{1-\epsilon^2} \cong 1 - \frac{h}{a},$$

$$1 - \frac{1}{2}\epsilon^2 \simeq 1 - \frac{h}{a}. \qquad \text{(II-10)}$$

$$\epsilon \cong \sqrt{\frac{2h}{a}}$$

This relation sets an estimate to the lowest value that the lower limit of the integral in Equation (PI-8) can have. Unfortunately, for sufficiently small h, the use of this estimate for ϵ yields physically unacceptable results; namely, that the average scattered power can be larger than the direct power. However, further thought suggests some way out of the difficulty. The lower limit, ϵ arises from that part of the scattering surface which is very near grazing. But that part of the surface would be very substantially shadowed by the roughness. One might, therefore, postulate rather reasonably that only part of the surface which receives rays at angles above the rms slope of the rough surface can contribute to the average scattered power. Conversely, this means that part of the surface which is near the grazing angle and receives rays from angles less than the rms slope is so heavily shadowed that very little energy is received (or scattered) there.

With the aid of Figure II-4 and some geometrical considerations, a reasonable estimate can be made for ϵ using the above considerations. From Figure 11-4 and the law of sines:

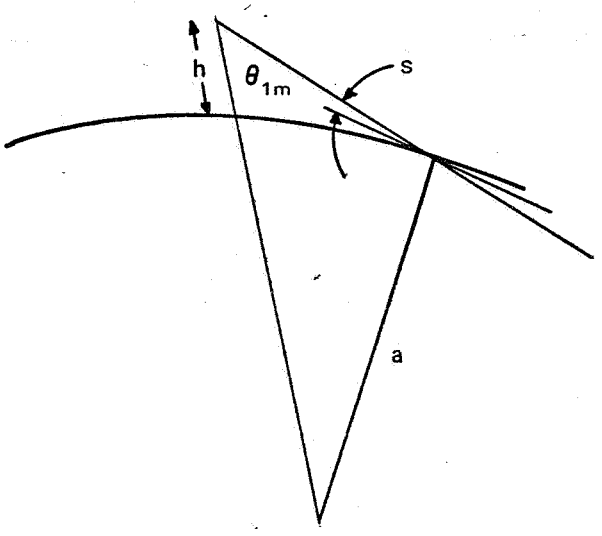

Figure II-4. Geometry for Estimating Shadowing Near Grazing Angles

$$\frac{\sin(s+\frac{\pi}{2})}{a+h} = \frac{\sin\theta_{1m}}{a}$$

$$\frac{\cos s}{1+h/a} = \sqrt{1-\cos^2\theta_{1m}} \qquad \text{(II-11)}$$

$$\left(1 - \frac{s^2}{2}\right)\left(1 - \frac{h}{a}\right) \simeq 1 - \frac{1}{2}\epsilon^2$$

or $$= \sqrt{s^2 + 2h/a}$$

This particular formula suggests that there exists a lower limit to ϵ even as $h \to 0$. From radar measurements of the lunar and Martian surface, it has been estimated that s lies between about 4° and 7°. Chdosing s = 0.1 (≈5.7°), E was calculated from Equation (II-11), and that value of ϵ was inserted into Equation (II-8). The results from numerical integration of Equation (II-8) are plotted in Figures II-5, -6, and -7, where, for purposes of estimating the Fresnel reflection coefficient of the Martian surface, it was assumed that $\varepsilon = 3$ and $\sigma = 0$.

2. Interpretation of Results

It must be admitted that it is very difficult to draw a firm conclusion from the results presented in Figures 11-5 through II-7. In fact, it appears that there exists a fundamental defect in the scattering formula, a defect which makes the whole computation for average scattered power quite suspect. It was decided to study this problem in greater detail. Reference is made to Equations (II-1) and (II-3) and Figure II-1. In this report, $P_Q\, dS$ represents the average power scattered

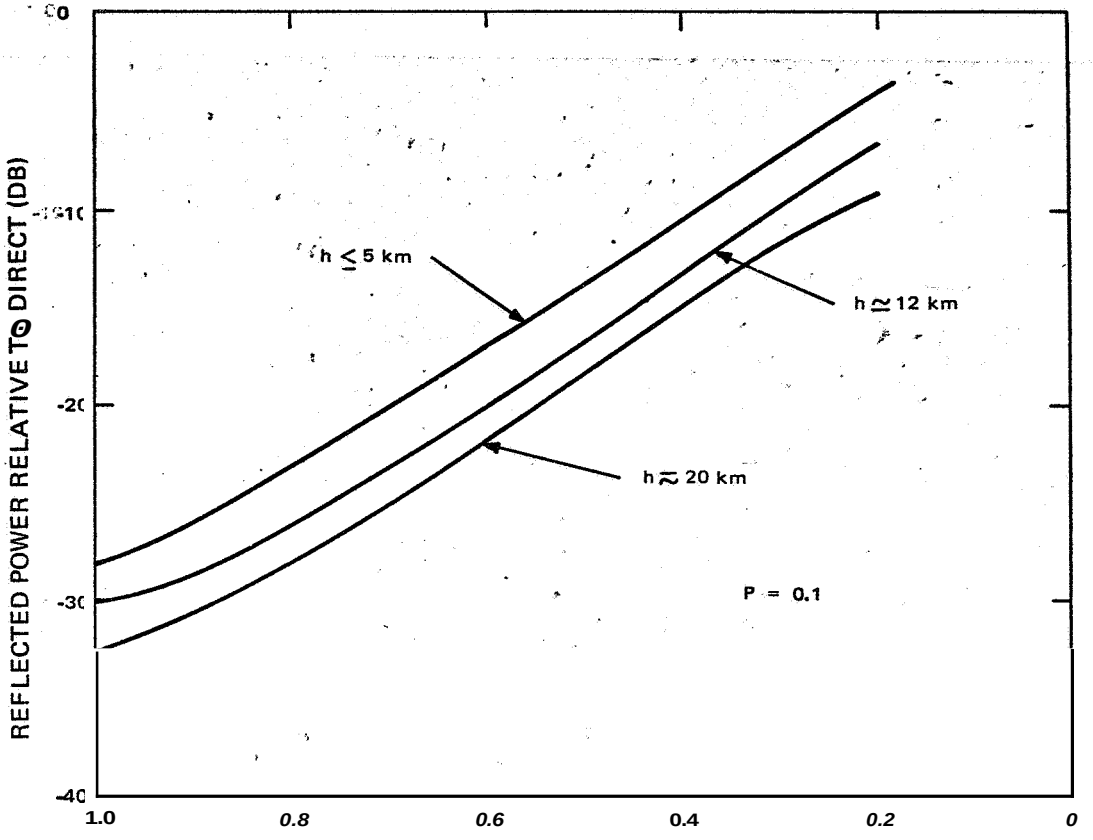

(a) VERTICAL POLARIZATION ($\cos\theta_2$)

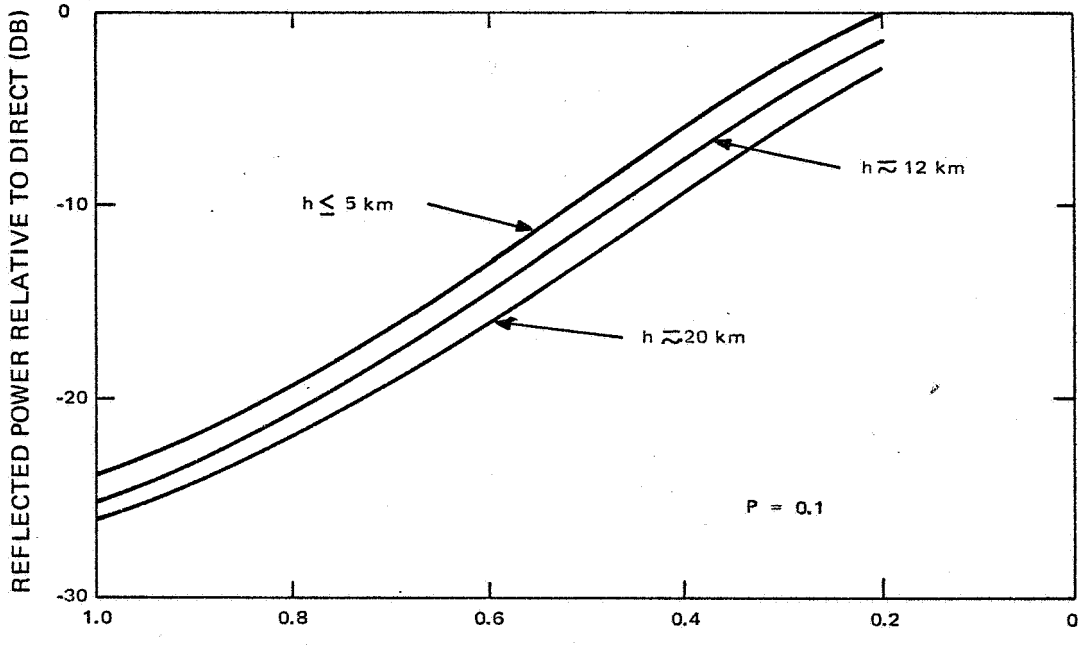

(b) HORIZONTAL POLARIZATION ($\cos\theta_2$)

Figure II-5. The Results of Integrating Equation 11-8 to Obtain the Average of Scattered Power for p = 0.1

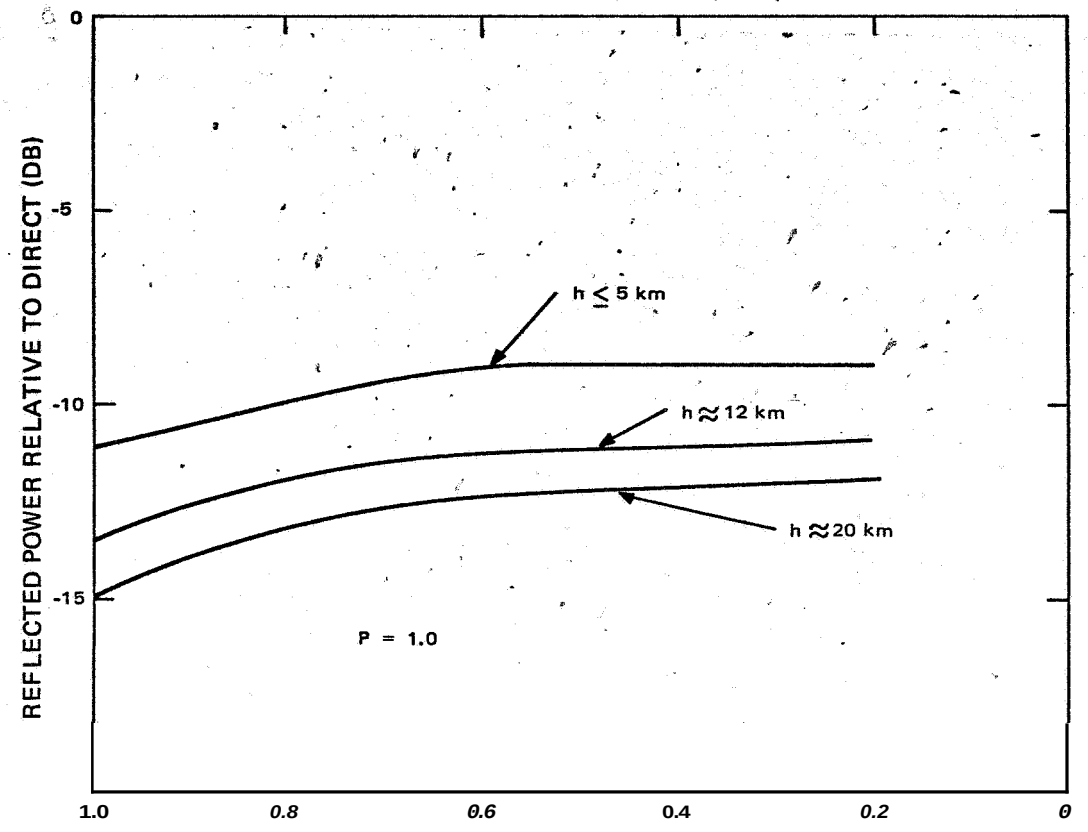

(a) VERTICAL POLARIZATION (COS θ_2)

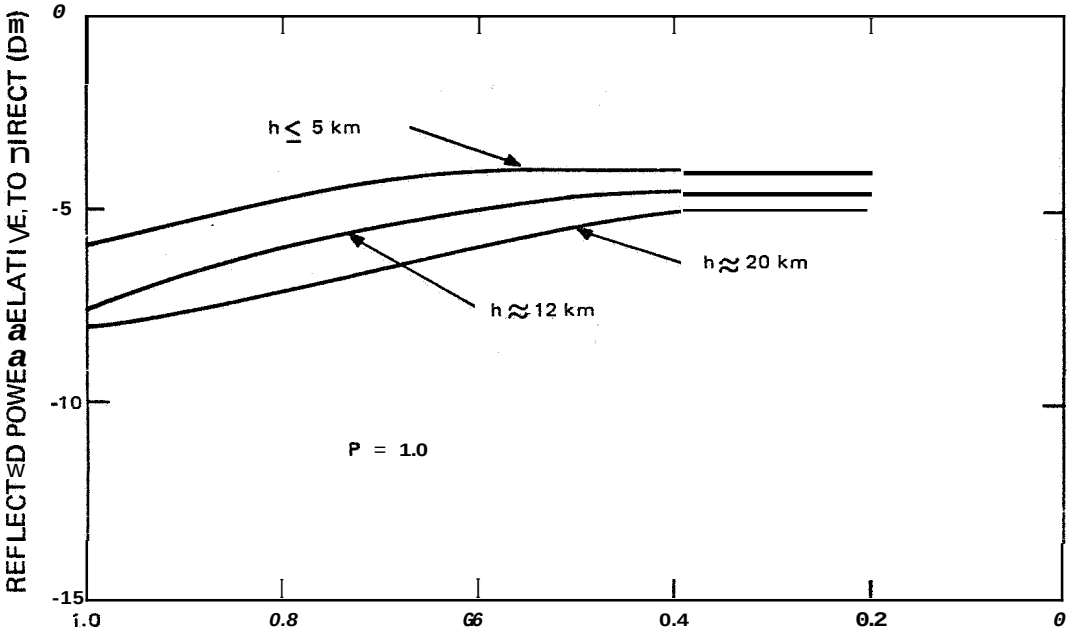

(b) HORIZONTAL POLARIZATION (COS θ_2)

Figure **11-6.** The Results of Integrating Equation II-8 to Obtain the Average Scattered Power for p = **1.0**

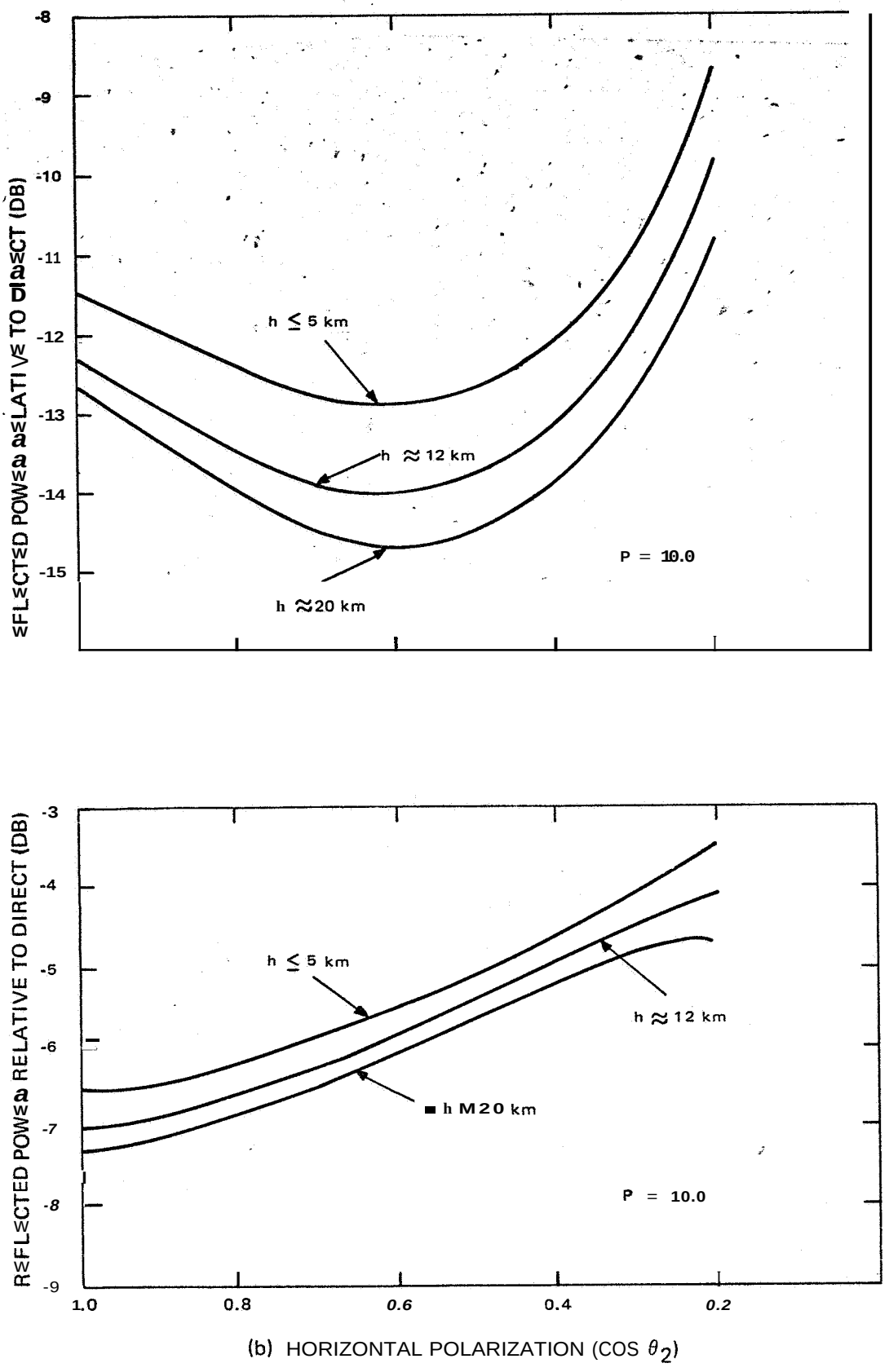

(b) HORIZONTAL POLARIZATION (COS θ_2)

Figure II-7. The Results of Integrating Equation II 8 to Obtain the Average Scattered Power for $\mathbf{p} = 10.0$

by an element of surface, dS, divided by the power in the direct beam. The direct beam has a power flux density $P_d \simeq \frac{1}{r^2}$, while the beam incident on the surface element dS is $P_i \simeq \frac{1}{r_1^2}$. Therefore, the power scattered by a perfectly reflecting surface element, dS, relative to the power in the incident beam is

$$P_o \frac{P_d}{P_i} dS = \frac{dS}{r_2^2} F(\theta_1,\theta_2,\varphi) \qquad \text{(IS-12)}$$

$$F(\theta_1,\theta_2,\varphi) = \frac{p^2}{2\pi} \frac{[1+\cos\theta_1\cos\theta_2-\sin\theta_1\sin\theta_2\cos\varphi]^2}{(\cos\theta_1+\cos\theta_2)^6 [1 + p^2f^2]^{3/2}}$$

and f^2 has already been defined in Equation **(11-3).** From conservation of power considerations, a requirement must be imposed on the function F; namely,

$$dS \iint \frac{F(\theta_1,\theta_2,\varphi)}{r_2^2} r_2^2 \sin\theta_2 d\theta_2 d\varphi = \cos\theta_1 \, dS \qquad \text{(II-13)}$$

Equation. (II-13) is the mathematical statement that the total power scattered over all directions by a perfectly reflecting surface element [given by the left side of Equation (II-13)] must be equal to the incident power intercepted by the surface element dS [given by the right side of Equation (II-13)]. In addition to the conservation of power requirement specified by Equation (II-3), reciprocity considerations impose another important constraint; namely, 'that the function, F, be an even function of φ and symmetric in θ_1 and θ_2 [i.e., $F(\theta_1, \theta_2, \varphi) = F(\theta_2, \theta_1, -\varphi)$].

This constraint imposed by reciprocity means that if Equation (11-13) is not automatically satisfied, it is probably not possible (except fortuitously) to find a "fudge factor" which would make the resulting scattering function satisfactory from both points of view-symmetry and conservation of power.

The integral on the left side of Equation (II-13) was evaluated with the aid of a computer and is identified as $N(\theta_1)$. Figure 11-8 presents a comparison of $N(\theta_1)$ with the required result, $\cos\theta_1$. It can be seen that for $p \leq 1.0$, $N(\theta_1)$ does not look like $\cos\theta_1$ at all. For $p = 10.0$, the effective scattering region tends to be reasonably concentrated around the specular point, and $N(\theta_1)$ begins to have some general resemblance to $\cos\theta_1$. Out of desperation, it was decided to modify the previous $F(\theta_1, \theta_2, \varphi)$ by multiplying F by a "fudge factor" $\cos\theta_1 \cos\theta_2$. This leaves the scattering function symmetric, but the requirement imposed by Equation (II-13) now becomes

$$\iint \cos\theta_2 \, F(\theta_1, \theta_2, \varphi) \, \sin\theta_2 \, d\theta_2 \, d\varphi = 1 \qquad \text{(TI-14)}$$

This integral was also evaluated on a computer and is presented in Figure If-9 as $M(\theta_1)$. It can be seen that $M(\theta_1)$ is not a constant as required. One must conclude, therefore, that the diffuse scattering function used in this analysis is not satisfactory for evaluating the average scattered power (or the fading rates) from an extended area. There is a fundamental defect in the scattering function unless $p > 10$, and no reasonable amount of "fudging" can doctor it up. Perhaps this is because there is an inherent inconsistency in the whole theory when an exponential correlation

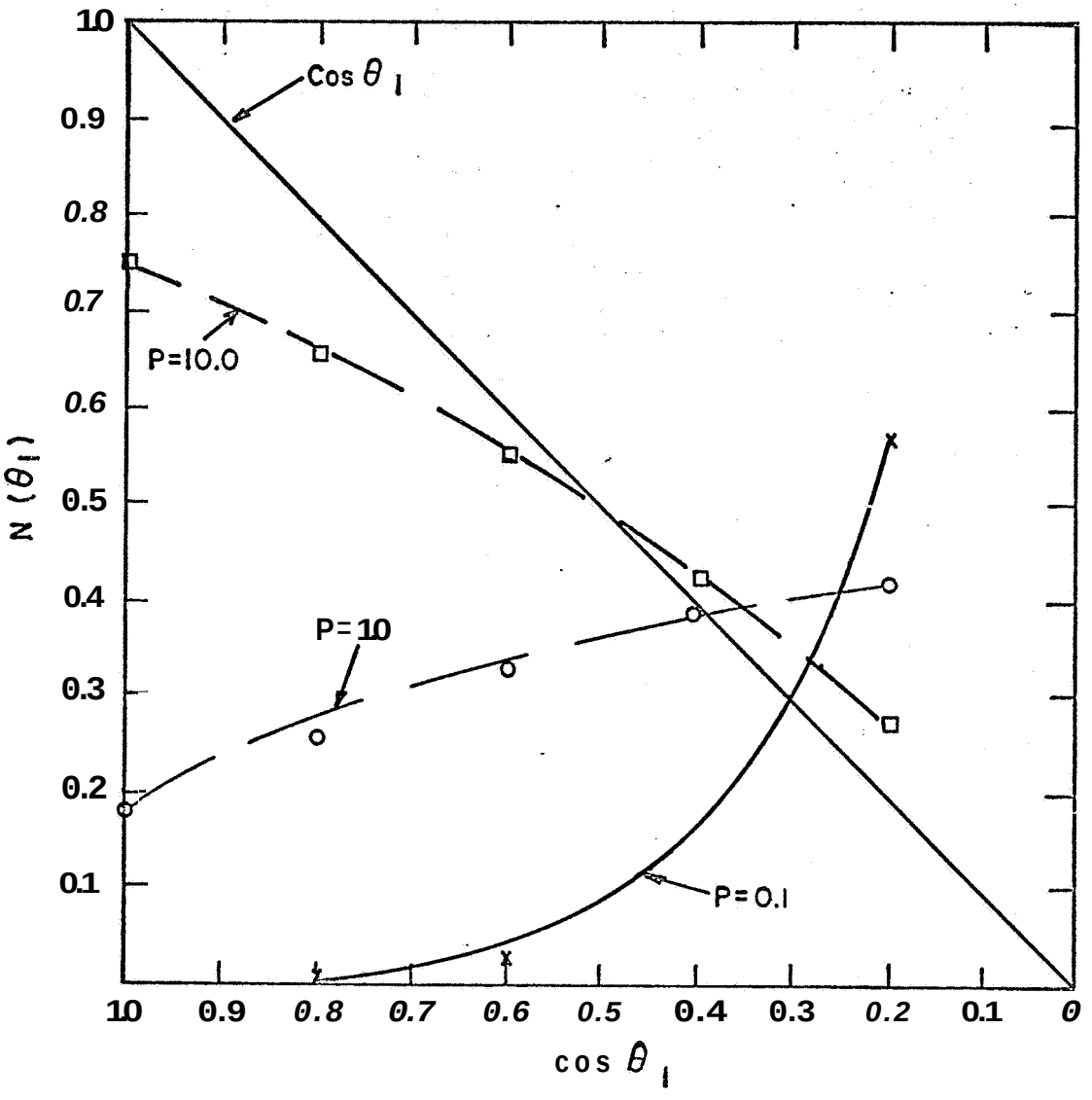

Figure II 8. A Comparison of N (θ_1) with *Cos* θ_1 (From Equation 11–13)

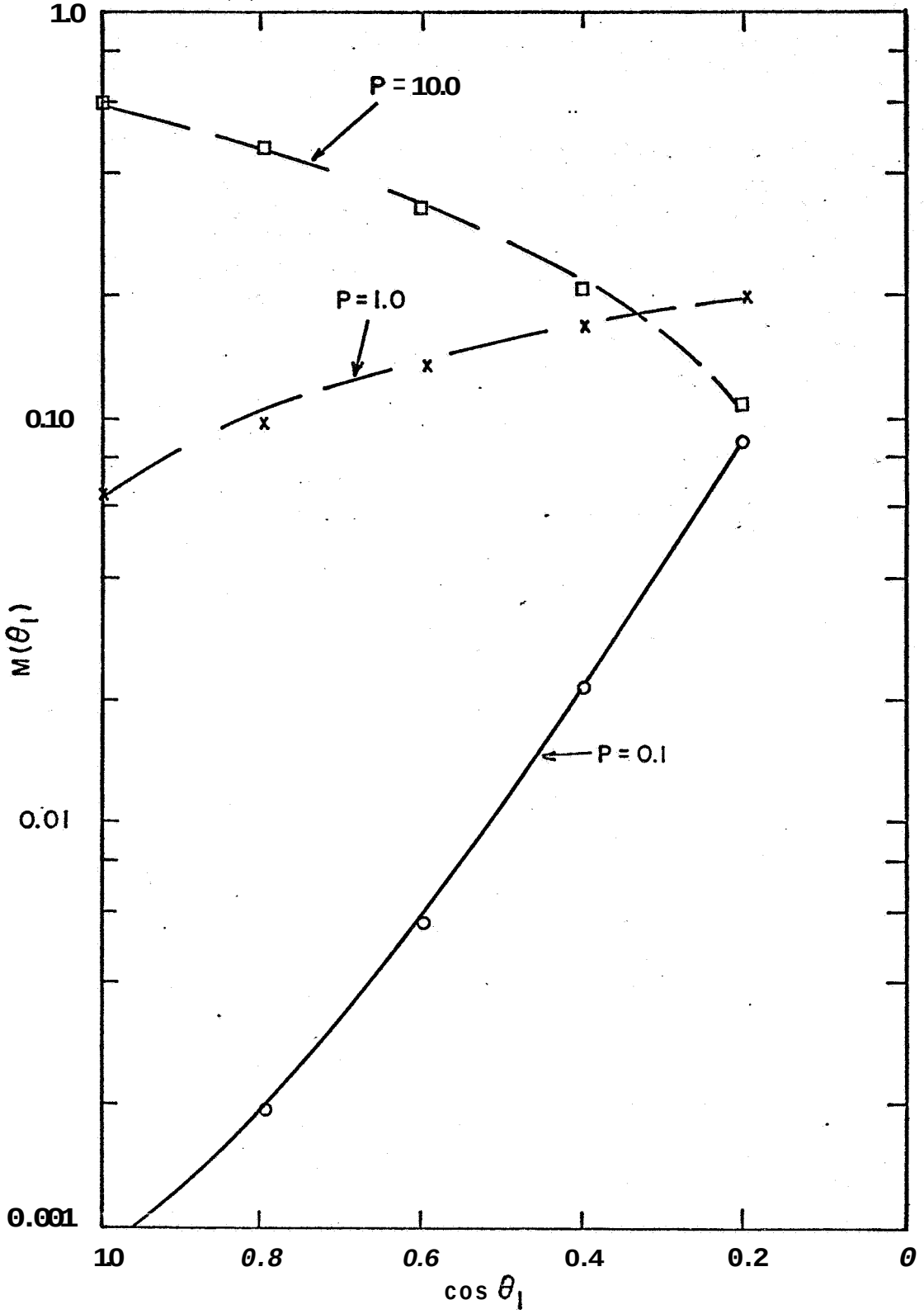

Figure II-9. A Comparison of M (θ_1) with *Cos* θ_1 (From Equation II-14)

function is assumed; namely, when the scattering function is derived based on a formulation for single scattering, the final result is a diffuse scattering function, which implies multiple scattering.

It is of importance to note that the earlier study on scattering' involving as it does highly directive scattering does satisfy both symmetry and conservation of power requirements as specified for Equation **(11-13).**

C. REFERENCES

1. "Selected Studies of VHF/UHF Communications for Planetary (Mars/Venus) Relay Links," RCA Final Report prepared for NASA, Ames Res. Center, under Contract No. NAS 2372 (See, in particular, section describing Task V).

2. Beckmann, P. and A. Spizzichino, "The Scattering of Electromagnetic Waves from Rough Surfaces," Pergamon Press, McMillan Co., New York 1963.

3. Beckmann, P., "Scattering by Composite Rough-Surfaces," Proc. IEEE, Vol. 53, pp. 1012-1015, Aug. 1965.

4. Harton, C. W., et al, "Model Studies on the Scattering of Acoustic Waves from a Rough Surface," J. Acoust. Soc. Am., Vol. 41, pp. 635-643, April 1966.

5. Middleton, D., "An Introduction to Statistical Communication Theory," McGraw-Hill, New York 1960.

SECTION 111

EXPERIMENTAL INVESTIGATION OF FAST FADING

A. INTRODUCTION AND SUMMARY

The experiment described in this task is an extension of the work done in an earlier study,' "Selected Studies of VHF/UHF Communications for Planetary (Mars, Venus) Relay Links." In that study, an experiment was conducted to evaluate the performance of a wideband noncoherent binary FSK system under the following conditions:

- No fading in the presence of Gaussian noise;
- Slow Rician fading in the presence of noise; and
- Hardwire synchronization.

The objective of this task is to extend the perforniance evaluation for conditions of fast Rician fading with and without doppler offset. The mathematical model of the channel is identical to that in the earlier study and is shown in Figure 111-I. For this evaluation, the Rayleigh generator was operated at fading rates greater than the bit rate (i.e., the correlation of the Rayleigh-distributed signal becomes very small over a bit interval) and the reflected- and direct-signal center frequencies have been offset to simulate differential doppler.

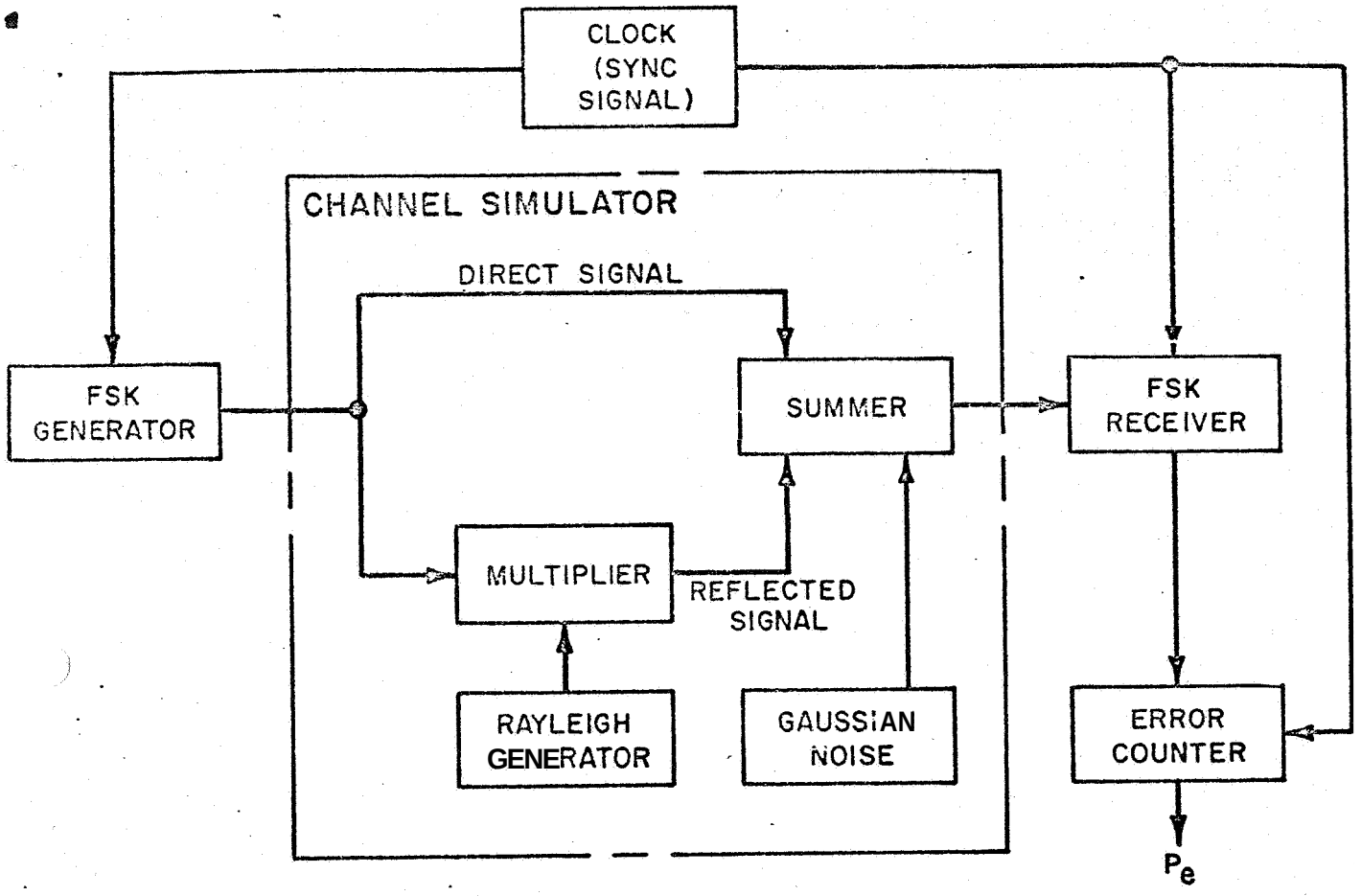

Figure III-1. Mathematical Representation of Ames Probe FSK Channel

The following basic results were obtained:

1. The effect of a reflected signal with a fading bandwidth smaller than the bit rate (slow fading) is to degrade the link performance relative to the no-multipath case. In terms of the mission, this means that if there are reflections from the planetary surface and the time-rate variation of the received reflected signal is slow relative to the bit time the link will be degraded.

2. The effect of increasing the fading bandwidth (for a constant reflected power) is to improve the link performance. The performance for fast fading (large fading bandwidth relative to bit rate) is superior to the no-multipath case. In terms of the mission, this means that fast fading does not degrade the link. However, the fact that the fast-fading signal may actually improve the performance cannot be utilized since at this time, the existence of a given magnitude signal can only be postulated, but not guaranteed.

3. The effect of an increasing frequency difference (differential doppler) between the reflected and direct signals is to improve link performance; the improvement is similar to that achieved by increasing the fading bandwidth. The impact of a differential doppler larger than the data rate is that the existence of multipath will not degrade the link. Again, since the existence of a large reflected signal can not be guaranteed, an improvement in link performance due to increasing doppler offset cannot be utilized.

4. The limit of improvement in link performance, due to fast fading, increasing doppler offset, or any combination of the two, is to consider the received signal energy as the sum of the direct and reflected energy.

B. EXPERIMENT IMPLEMENTATION

The equipment used in this experiment is similar to that employed in the original investigation? The only differences are the use of a fast-fading generator with provision for offsetting the reflected-signal center frequency from the direct-signal center frequency in place of the slow-fading generator. The experimental system block diagram, shown in Figure III-2, is the same for both experiments. A block diagram of the fast-fading generator is shown in Figure III-3.

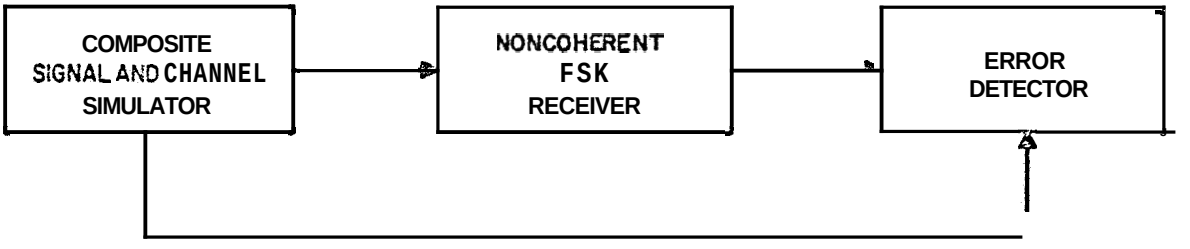

Figure III-2. Experimental System Block Diagram

The fast-fading generator operates on the principle that the envelope of a narrow-band noise signal centered about a carrier frequency is Rayleigh distributed[2]. To implement this principle, a wideband noise source was operated into a narrow-band filter centered at 100 kHz. The physical implementation consisted of a General Radio noise source and a Hewlett-Packard Model 310 Wave Analyzer.

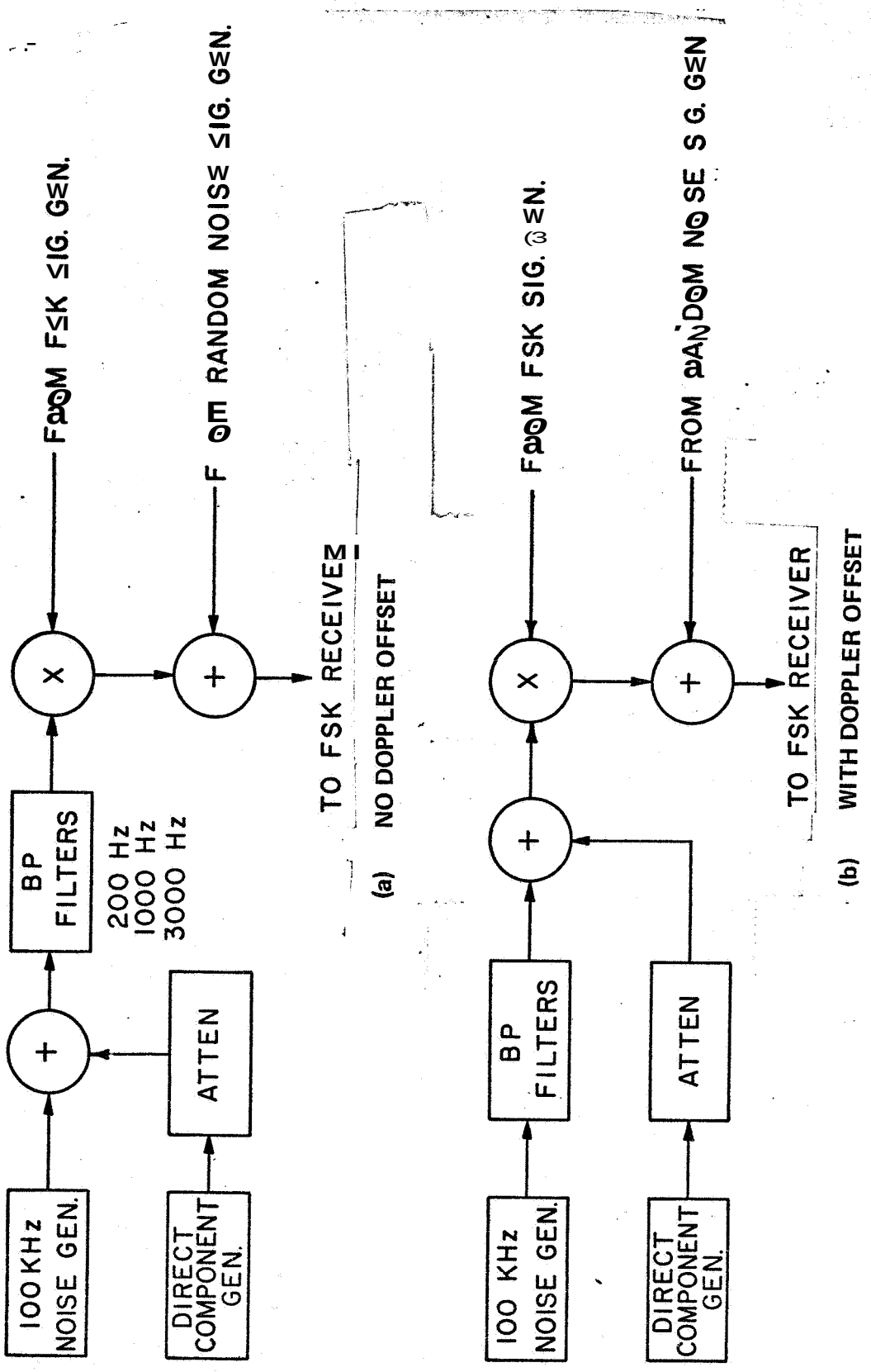

Figure III-3. Fast Fading Generator, Block Diagram

The wave analyzer had selectable bandwidths of 200, 1000, and 3000 Hz. This provided a variable-fading-bandwidth capability,

The signal at the output of the narrow-band filter can be represented by

$$S_R(t) = B_1 \sin \omega_R t + B_2 \cos \omega_R t, \qquad \text{(III-1)}$$

where ω_R is the center frequency of the bandpass filter (in radians per second).

$$\overline{B_1}^2 = \overline{B_2}^2 = P_R \qquad \text{(III-2)}$$

where

B_1^2 is the average value of the square of B_1, and

P_R is the average power of signal $S_R(t)$.

Then, $S_R(t)$ represents the reflected signal from the planetary surface with a power P_R and a carrier frequency ω_R. The envelope of $S_R(t)$ is Rayleigh distributed.

The direct signal can be represented as

$$S_D(t) = A \sin \omega_D t \qquad \text{(III-3)}$$

where the power of the direct signal is

$$P_D = \frac{A^2}{2}. \qquad \text{(III-4)}$$

Then, the sum of $S_R(t) + S_D(t)$ corresponds to the total signal received, or

$$\Sigma S_R(t) + S_D(t) = A \sin \omega_D t + B_2 \cos \omega_R t + B_1 \sin \omega_R t \qquad \text{(III-5)}$$

We can write

$$\omega_R = \omega_D + \omega_B \qquad \text{(III-6)}$$

where ω_B corresponds to the offset frequency between the direct and reflected signals.

Now,

$$\begin{aligned} \Sigma S_R(t) + S_D(t) &= A \sin \omega_D t + B_1 \sin (\omega_D + \omega_B)\, t + \\ &\quad B_2 \cos (\omega_D + \omega_B)\, t \\ &= [A + B_1 \cos \omega_B t + B_2 \sin \omega_B t] \sin \omega_D t + \\ &\quad [B_2 \cos \omega_B t - B_1 \sin \omega_B t] \cos \omega_D t \end{aligned} \qquad \text{(III-7)}$$

The envelope of this expression is

$$E(t) = \sqrt{A^2 + B_1^2 + B_2^2 + 2AB_1 \cos \omega_B t + 2AB, \sin \omega_B t} \qquad \text{(III-8)}$$

For the case where there is no offset, ω_B equals zero; then

$$E_o(t) = \sqrt{A^2 + B_1^2 + B_2^2 + 2AB_1} \qquad \text{(III-9)}$$

The envelope distribution is Rician[3] where the reflected power is considered as noise power in Reference 3.

The ratio of direct to reflected power (γ^2) is from Equations III-2 and III-4.

$$\gamma^2 = \frac{P_D}{P_R} = \frac{A^2}{2\bar{B}_1^2} = \frac{A^2}{\bar{B}_1^2 + \bar{B}_2^2} \qquad \text{(III-10)}$$

The distribution is discussed by Schwartz[4] as a function of γ^2, where in his discussion, γ^2 would be the signal-to-noise power ratio. Where $\gamma^2 = 0$, the distribution becomes Rayleigh and as $\gamma^2 >> 1$, the distribution approximates a Gaussian distribution about the amplitude A with a variance $\bar{B}_1^2$.

The output of the fast-fading generator for several values of fading bandwidths and γ^2 is shown in Figure III-4. These photographs were taken from an oscilloscope connected to the output of the bandpass filter shown in Figure III-3a. The wave analyzer (bandpass filter) was operated in the automatic-frequency-control mode which locks the center of the bandpass to the frequency at the input, thus ensuring that the offset between the direct and reflected signals is zero. The signal at this point is not frequency shift keyed (FSK). The direct component power was held constant in all photographs except for $\gamma^2 = 0$, where the reflected power was made equal to the direct power in the other photos (direct power is zero for $\gamma^2 = 0$). The vertical and horizontal scales are constant throughout the sequence,

Observing any horizontal set of Figure III-4, it is seen that the amplitude distribution is about the same for all three bandwidths but that the time distribution varies with bandwidth. This is expected, since Equation III-9 shows that the

Figure III-4. Fading Simulator Output Waveforms (No Loppler Offset)

amplitude distribution is only a function of the powers of the direct and reflected signals and not of their bandwidths. An important aspect to note is that for the experiments conducted here, the bit time was 10 milliseconds and that as the bandwidth is increased, a larger number of amplitude variations occur within a bit period. This means that if the envelope amplitude is averaged over the bit period, more independent samples of the waveform are obtained for the larger bandwidths and the measured average value tends to approach the true average value with a higher probability. In mathematical terms,

$$\frac{1}{T}\int_{0}^{T} E(t)\,dt = \bar{E} \text{ as } B >> \frac{1}{T} \qquad (111\text{-}11)$$

where $\bar{E}$ is the average value of $E(t)$, B'is the fading bandwidth, and T is the bit period.

Observing the vertical sets of Figure III-4, as γ^2 increases, the magnitude of the amplitude variations tend to decrease. When $\gamma^2 >> 1$, the distribution tends to become Gaussian about the direct-signal amplitude, **A,** and the variance approaches the square root of the reflected power, $\sqrt{B_1^2}$.

The effect of frequency offset between the direct and reflected signals is shown in Figure III-5 for $\gamma^2 = 1$, and B = 200 **Hz.** The basic equation describing the envelcpe for this case is Equation III-8.

$$E(t) = \sqrt{A^2 + B_1^2 + B_2^2 + 2A\left[B_1 \cos \omega_B t + B_2 \sin \omega_B t\right]}$$

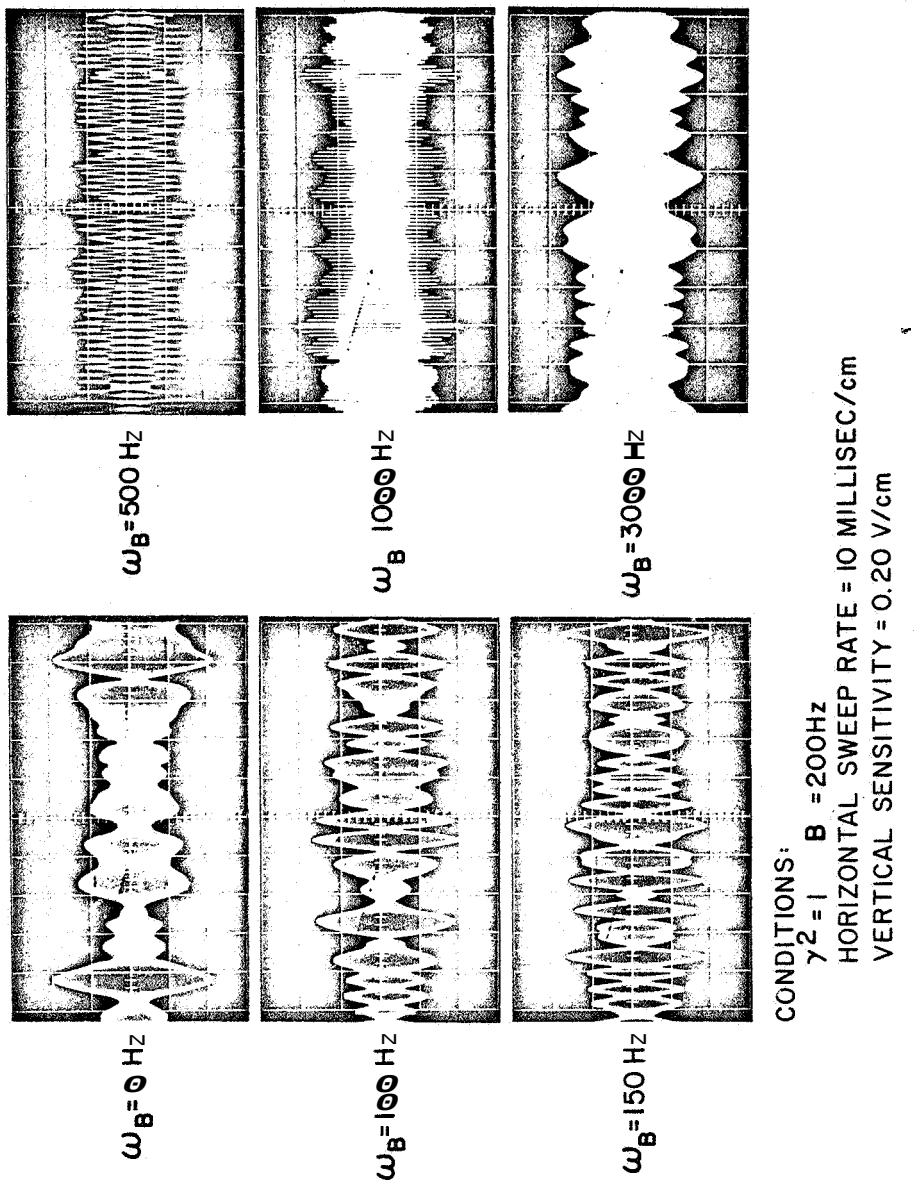

Figure III-5. Fading Simulator Output Waveforms (with Doppler Offset)

When $\omega_B >> B$ (the fading bandwidth), the term $B_1 \cos \omega_B t + B_2 \sin \omega_B t$ becomes a narrow-band Gaussian distribution centered about ω_B (B_1 and B_2 are each independent Gaussian variables) and can be written as

$$B_1 \cos \omega_B t + B_2 \sin \omega_1 t \simeq Q \sin (\omega_B t + \theta), \qquad \text{(In-12)}$$

where $Q = \sqrt{B_1^2 + B_2^2}$ (Rayleigh distributed), and θ is a random variable with all values equally likely for $0 < B < 2\pi$. Thus, Equation III-8 can be written as

$$E = \sqrt{A^2 + Q^2 + 2AQ \sin (\omega_B t + \theta)} \qquad \text{(111-13)}$$

The $2AQ \sin (\omega_B t + \theta)$ component can readily be seen in Figure III-5 for ω_B = 500 Hz and ω_B = 1000 Hz. For ω_B = 3000 Hz, the horizontal time scale does not allow resolution of the offset frequency. If only the envelope of the 2AQ sin $(\omega_B t + 6)$ component is considered (as in fact occurs in the ω_B = 3000 Hz photograph of Figure 111-5) then the overall envelope is

$$E = \sqrt{A^2 + Q^2 + 2AQ} \quad \text{or} \quad E = A + Q \qquad \text{(III-14)}$$

which is a constant (A) plus a Rayleigh variable (Q). By observing the ω_B = 3000 Hz recording in Figure 111-5, the appearance is as predicted. A Rayleigh waveform is shown for comparison in Figure III-4 (γ^2 = 0) without the constant A.

A detailed block diagram of the equipment implementation employed in the tests is shown in Figure III-6, with an equipment chart. The FSK receiver is the same as employed in the original study' and is described in detail in the final report.

Figure III-6. Equipment Implementation Block Diagram

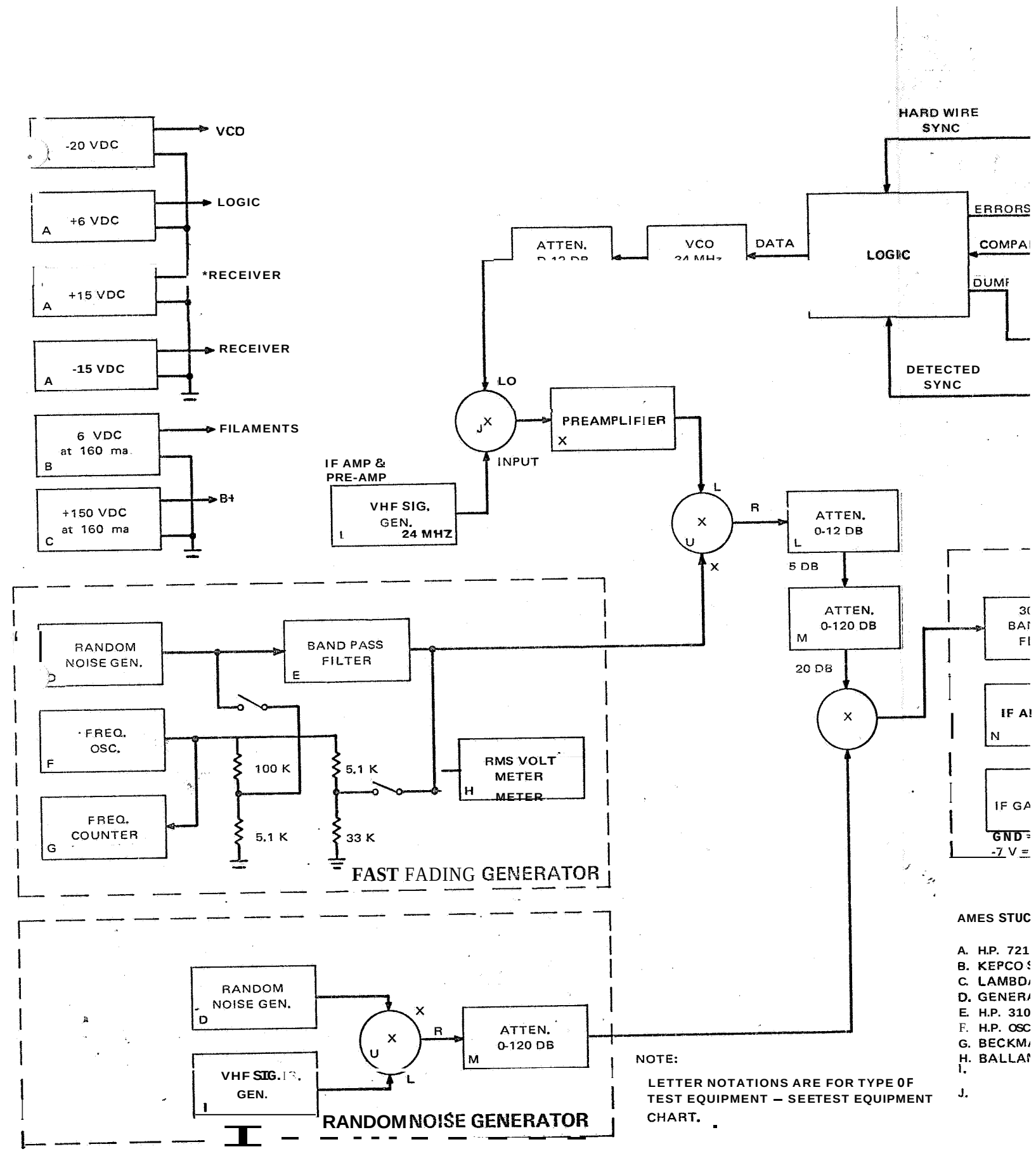
-20 VDC
VCO
+6 VDC
A
LOGIC
+15 VDC
A
*RECEIVER
-15 VDC
A
RECEIVER
6 VDC
at 160 ma
B
FILAMENTS
+150 VDC
at 160 ma
C
B+
HARD WIRE
SYNC
ATTEN.
VCO
24 MHz
DATA
LOGIC
ERRORS
COMPA
DUMP
DETECTED
SYNC
LO
INPUT
PREAMPLIFIER
X
IF AMP &
PRE-AMP
VHF SIG.
GEN.
24 MHZ
I
L
R
U
X
ATTEN.
0-12 DB
L
5 DB
ATTEN.
0-120 DB
M
20 DB
X
RANDOM
NOISE GEN.
D
BAND PASS
FILTER
E
FREQ.
OSC.
F
100 K
5.1 K
RMS VOLT
METER
H
METER
FREQ.
COUNTER
G
5.1 K
33 K
FAST FADING GENERATOR
RANDOM
NOISE GEN.
D
X
U
X
R
L
ATTEN.
0-120 DB
M
VHF SIG.
GEN.
I
RANDOM NOISE GENERATOR
AMES STUC
A. H.P. 721
B. KEPCO
C. LAMBDA
D. GENERA
E. H.P. 310
F. H.P. OSC
G. BECKMA
H. BALLAN
I.
J.
NOTE:
LETTER NOTATIONS ARE FOR TYPE OF
TEST EQUIPMENT — SEETEST EQUIPMENT
CHART.

FIG III-6-1

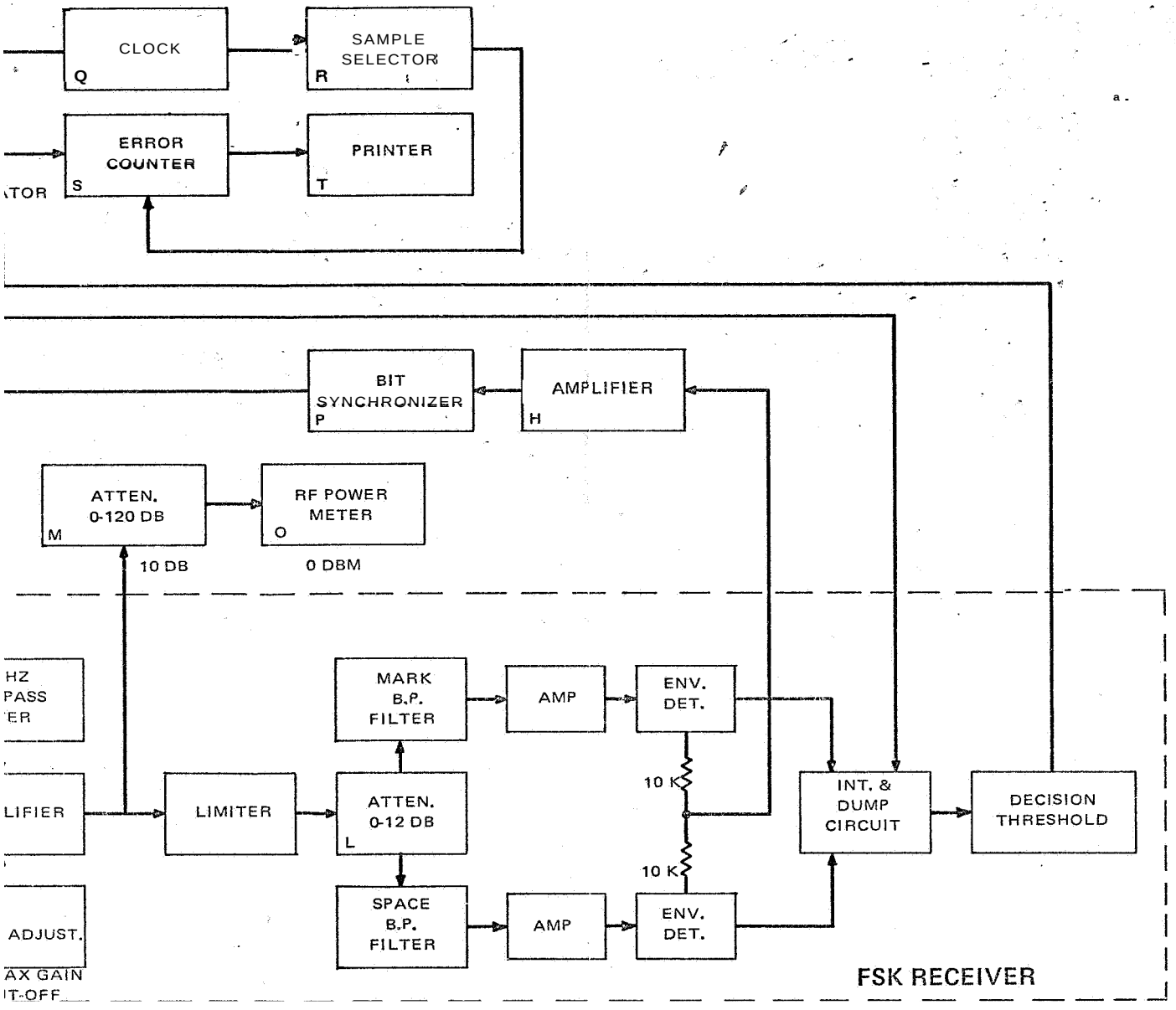

PROGRAM TEST EQUIPMENT CHART

OWER SUPPLY
32-5 POWER SUPPLY
-881M POWER SUPPLY
RADIO RANDOM NOISE GEN. 1390-B
VAVE ANALYZER
00 CD
E FUT METER – 7150 COUNTER
NE RMS VOLTMETER MODEL 320
/HF SIG. GEN.
N. RADIO GR-874

K. PRE-AMP RHG ELECTRONICS MODEL F1003R
L. ATTENUATOR H.P. VHF MODEL 355A, 0-12 DB
M. ATTENUATOR H.P. UHF MODEL 355B, 0-120 DB
N. 10 MHZ IF AMP. RHF ELECTRONICS MODEL E 1002 PM
O. R.F. POWER METER H.F. MODEL 431A
P. BIT SYNCHRONIZER – TELEMETRICS MODEL 6203A
Q. GASL PULSE & SQUARE WAVE GEN. MODEL PSQ-1
R. BECKMAN PRESET COUNTER MODEL **7426**
S. BECKMAN/BERKELEY UNIVERSAL E PUT AND TIMER MODEL 7360
T. BECKMAN PRINTER MODEL 1453
U. MIXER – HP. MODEL 10514A

Fig. III-6

C. EXPERIMENTAL RESULTS

1. General

The results of the experiment determine the effects of fast fading (with and without doppler offset of the reflected signal) on a wideband noncoherent FSK system. The mathematical analysis in the previous paragraph is now continued to determine the effects of slow fading and fast fading on the FSK system. The analysis is carried out sufficiently to qualitatively describe the effects of fading on the FSK system as a function of the pertinent fading parameters, i.e, , fading bandwidth, ratio of direct signal power to reflected power (γ^2), and doppler offset. The mathematical analysis is presented in order to provide a background to evaluate the experiment,

2. Mathematical Analysis

An assumption implicit in all the analysis and experimental data is that the time delay between a bit arriving at the receiver along the direct path and one along the reflected path is negligible compared to the bit period. The low bit rates and the flight geometry for the missions considered justify this assumption.

The envelope of the incoming signal is described in Equation III-8 as

$$E(t) = \sqrt{A^2 + B_1^2 + B_2^2 + 2A\ B_1 \cos \omega_B t + 2AB_2 \sin \omega_B t}$$

For the case where WT is large, it was shown in Reference 1 (Section III (E)) that the signal output of the envelope detector is proportional to the square of

its input and that the noise power output is a constant. Therefore, the signal at the output of the detector can be written as

$$E'(t) = K(A^2 + B_1^2 + B_2^2 + 2AB_1 \cos \omega_B t + 2AB_2 \sin \omega_B t) \qquad \text{(In-15)}$$

where K is a detector constant.

The integrate and dump circuit (matched filter) performs the operation of averaging the signal over a bit period so that

$$\bar{E}' = \frac{K}{T} \int_0^T (A^2 + B_1^2 + B_2^2 + 2AB_1 \cos \omega_B t + 2AB_2 \sin \omega_B t)dt \qquad \text{(III-16)}$$

The noise output of the same circuit is

$$\bar{N}' = \frac{K}{T} \int_0^T N\,dt \qquad \text{(In-17)}$$

where N is a Gaussian distributed noise variable. The output signal-to-noise ratio is then

$$\frac{\bar{E}'}{\bar{N}'} = \frac{1}{T} \int_0^T \frac{(A^2 + B_1^2 + B_2^2 + 2AB_1 \cos \omega_B t + 2AB_2 \sin \omega_B t)\,dt}{\frac{1}{T} \int_0^T N\,dt} \qquad \text{(III-18)}$$

This is a general expression of performance as a function of fading bandwidth including doppler offset.

In order to evaluate the effects of different fading conditions, a parameter, ρ, is defined, which is the ratio of the signal-to-noise ratio in the link with

multipath present to the signal–to–noise ratio without multipath (all other conditions remaining constant). From Equation III-18, the signal–to–noise ratio with no multipath ($B_1 = B_2 = 0$) is

$$\frac{S}{N} = \frac{\frac{1}{T}\int_0^T A^2\,dt}{\frac{1}{T}\int_0^T N\,dt} - \frac{A^2}{\frac{1}{T}\int_0^T N\,dt} \qquad \text{(III-19)}$$

The ratio of S/N's with and without multipath from Equations III-18 and 111-19 is then

$$\rho = \frac{1}{T}\int_0^T \left(1 + \frac{B_1^2 + B_2^2}{A^2} + 2\,\frac{B_1}{A}\cos\omega_B t + 2\,\frac{B_2}{A}\sin\omega t\right) dt \qquad \text{(III-20)}$$

This is the generalized expression for ρ and the intent is to analyze it for the various cases of slow fading and fast fading with and without offset in order to provide a theoretical background for the experimental data obtained.

a. Case I: Slow Fading, No Doppler Offset

This is an experiment that was performed during the earlier study[1] and is reintroduced here in summary form for completeness and to emphasize the contrast between slow fading and fast fading.

B_1 and B_2 are random variables with Gaussian statistics. For slow fading, B_1 and B_2 can be considered constant during the bit period since $BT \ll 1$.

Therefore,

$$B_1^2 = \frac{1}{T}\int_o^T B_1^2\, dt$$

$$B_2^2 = \frac{1}{T}\int_o^T B_2^2\, dt \qquad \text{(III-21)}$$

$$B_1 = \frac{1}{T}\int^T B_1\, dt$$

$$\omega_B = 0 \quad \text{(nodoppler offset)}$$

For this case, p (from Equation **III-20)** reduces to

$$\rho_I = 1 + \frac{B_1^2 + B_2^2}{A^2} + \frac{2B_1}{A} \qquad \text{(III-22)}$$

and $\left|\frac{2B_1}{A}\right| > \frac{B_1}{A} + \left(\frac{B_2}{A}\right)$, p will be less than one and the performance of the link

b. Case II: Fast Fading, No Doppler Offset

In the case of very fast fading, B_1 and B_2 change rapidly over a bit period. Since B_1 and B_2 are Gaussian-distributed random variables, and their average value is zero, then

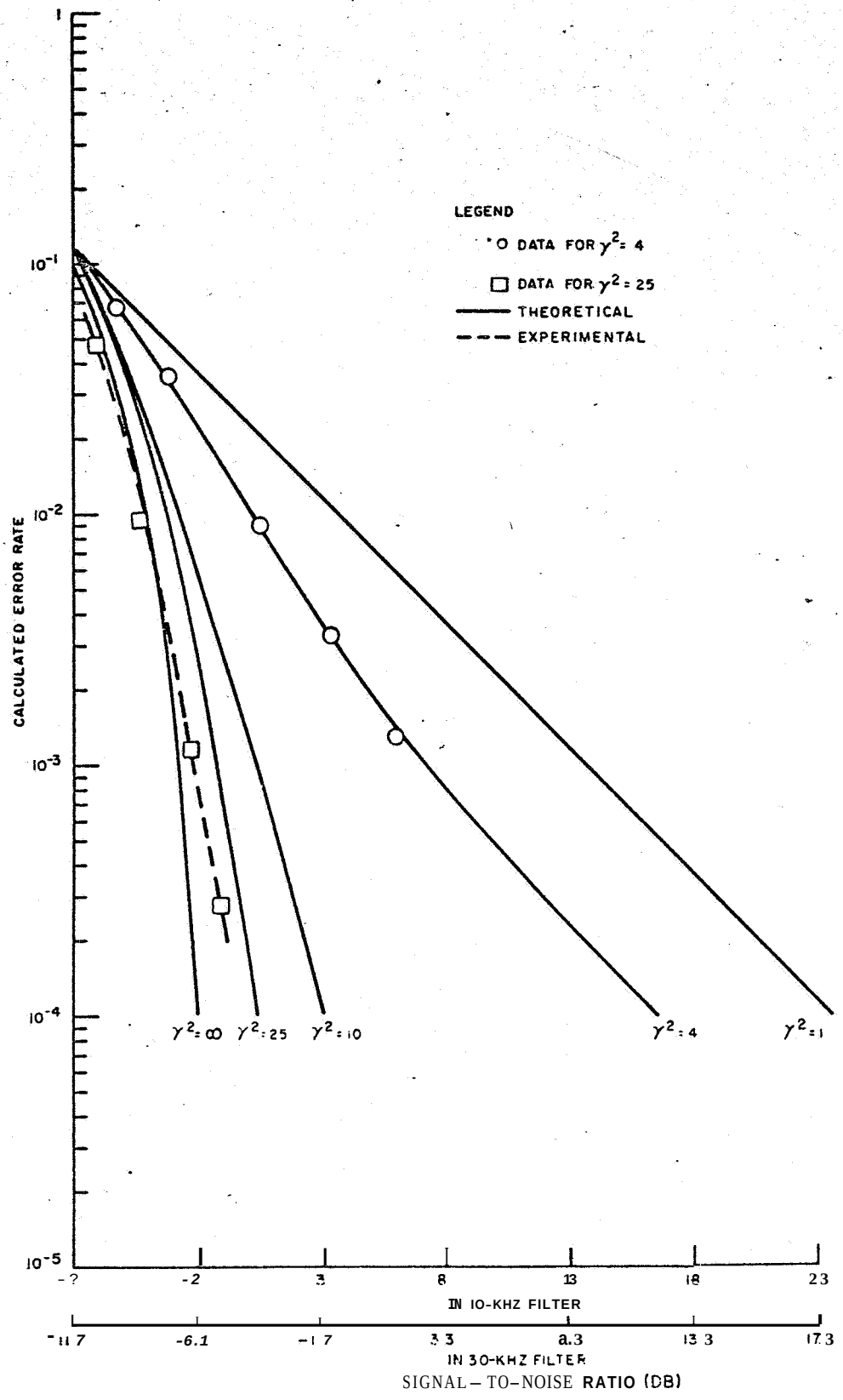

Figure III-7. Calculated Error Rates as a Function of S/N with γ^2 as a Parameter, No Limiter, Fading Conditions, and an Assumed Square-Law Detector

$$A\int_0^T B_1\,dt \rightarrow 0 \qquad A\int_0^T B_2\,dt \rightarrow 0$$

$$\int_0^T B_1^2\,dt \rightarrow \bar{B}_1^2 \qquad \int_0^T B_2^2\,dt \rightarrow \bar{B}_2^2 \qquad \text{(HI-24)}$$

$\omega_B = 0$ (no doppler offset)

For this case, ρ (from Equation III-20) reduces to

$$\rho_{II} = 1 + \frac{\bar{B}_1^2 + \bar{B}_2^2}{A^2} \qquad \text{(III-25)}$$

The ratio of direct signal power to reflected power (γ^2) is equal to $\frac{A^2}{\bar{B}_1^2 + \bar{B}_2^2}$, therefore, p can be written as

$$\rho_{II} = 1 + \frac{1}{\gamma^2} \qquad \text{(III-26)}$$

For fast fading, one would expect the link performance to be improved by the ratio ρ_{II} above. The improvement approaches ρ_{II} when BT approaches infinity, where B is fading bandwidth and T is bit period.

The experimental data for a fading bandwidth of 3,000 Hz are shown in Figure III-8. Since the data rate for these experiments is 100 bits per second, a 3000-Hz fading bandwidth corresponds to BT of 30. At $\gamma^2 = 1$, there should be an improvement over $\gamma^2 = \infty$ of 3 db, and at $\gamma^2 = 4$, an improvement of 1 db. For a mean error rate (P_e) of 10^{-3}, these predictions are realized, At error rates of 10^{-4} and 10^{-5}, the correspondence between prediction and experiment is not as good indicating that the fading bandwidth, B, needs to be larger to ensure that $\int_0^T B_1\,dt$ is small enough. The design center for this mission is a mean error rate of 10^{-3}.

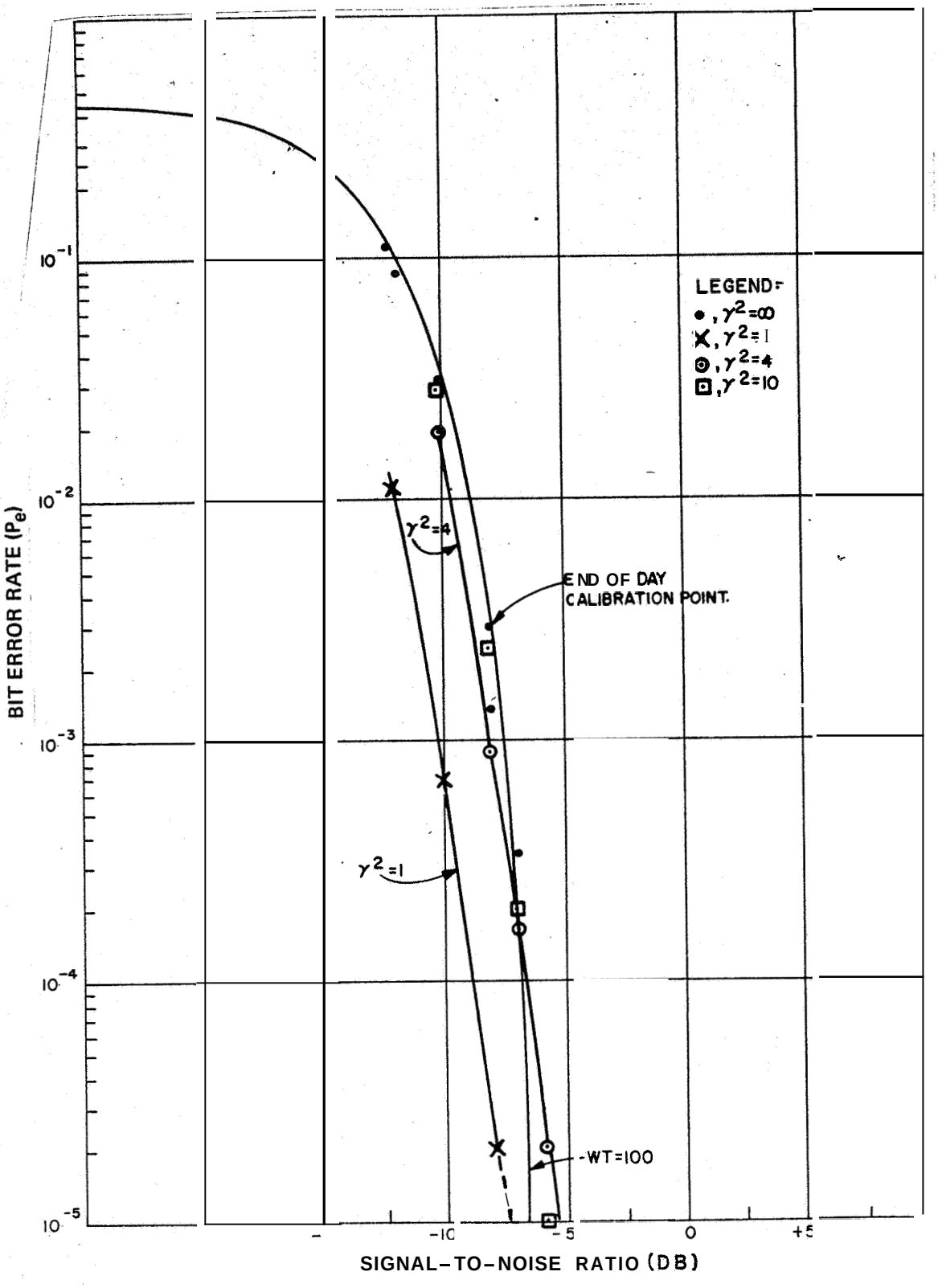

Figure III-8. Bit Error Rate as a Function of Signal-to-Noise Ratio and γ^2 for a Fading Bandwidth of 3 kHz (No Doppler Offset)

The experimental data for fading bandwidths of 200 Hz and 1000 Hz, which correspond to BT's of 2 and 10, respectively, are shown in Figures 111-9 and III-10. These curves show the degradation of link performance as B becomes small. Even though BT is small for the 200-Kz fading bandwidth, the performance is still far superior to the very slow fading case of Figure 111-7. The effect of BT (fading rate) on the error curves is indicated in Figure III-11, where a family of curves for various BT's are plotted for $\gamma^2 = 1$.

A set of data was taken for a bit rate of 1000 bits-per second and a fading bandwidth of 1000 Hz. This corresponds to a WT product of 10 and BT of 1. These curves are shown in Figure III-12. All previous data presented were taken at a WT product of 100. The bit error rate performance at WT = 10 is consistent with that taken at WT = 1000 and the same general trends are exhibited, as would be expected from the analysis.

The application of the data on fading to the mission requirements is perhaps best presented in the form of the penalty imposed by the presence of a reflected signal (rnultipath) as a function of BT. The mission design center is an error rate of 10^{-3}. Figure III-13 presents the margin required over an ideal link with no multipath to achieve an error rate better than 10^{-3}. From the previous multipath nnalysis, $\gamma^2 \geq 4$ can be achieved with an omnidirectional antenna aboard the probe by constraining the look angle from the probe to the spacecraft bus from the zenith to 60 degrees. Additionally, the slowest fading bandwidth,

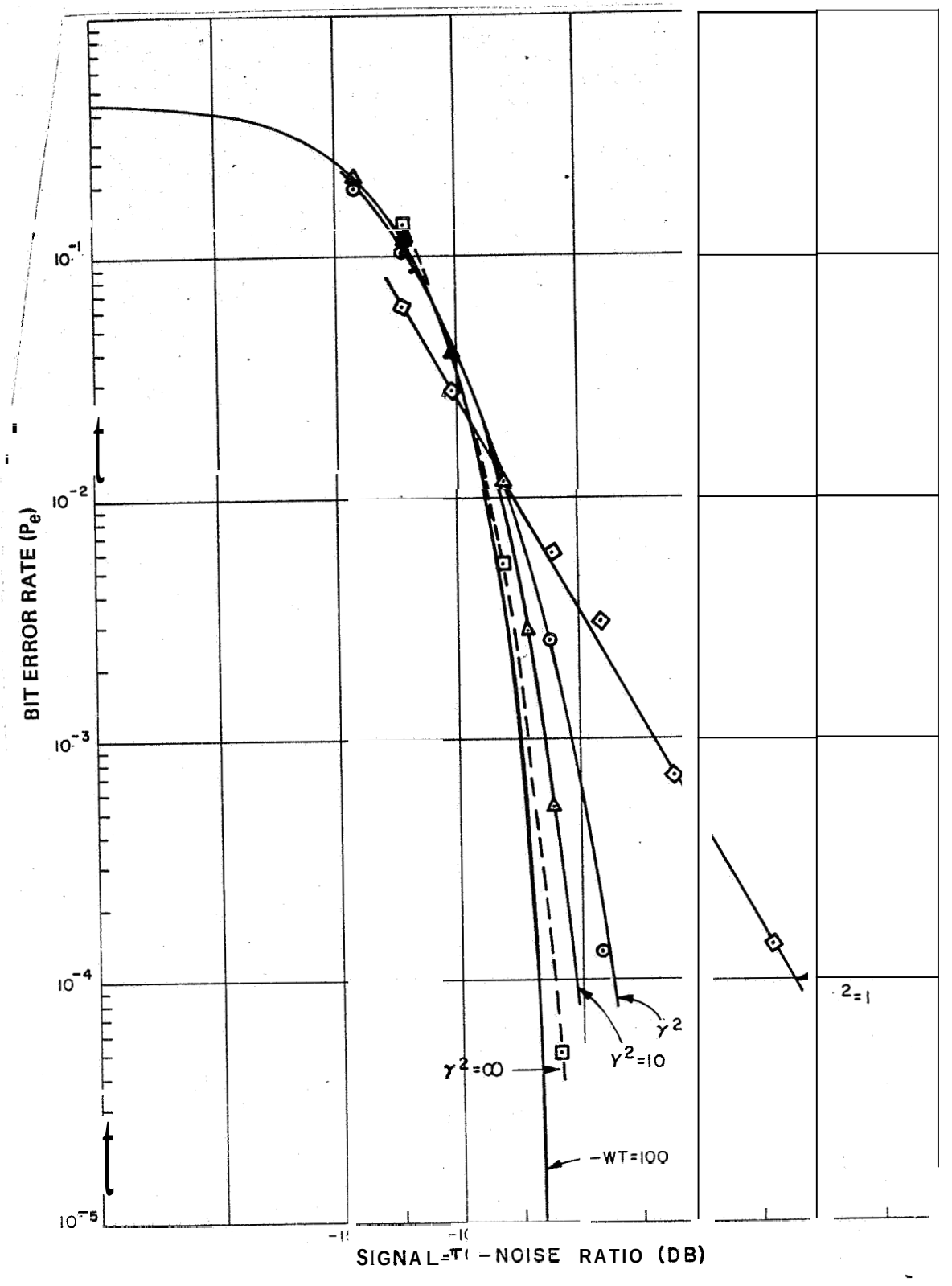

Figure III-9. Bit Error Rate as a Function of Signal-to-Noise Ratio and γ^2 for a Fading Bandwidth of 200 Hz (No Doppler Offset)

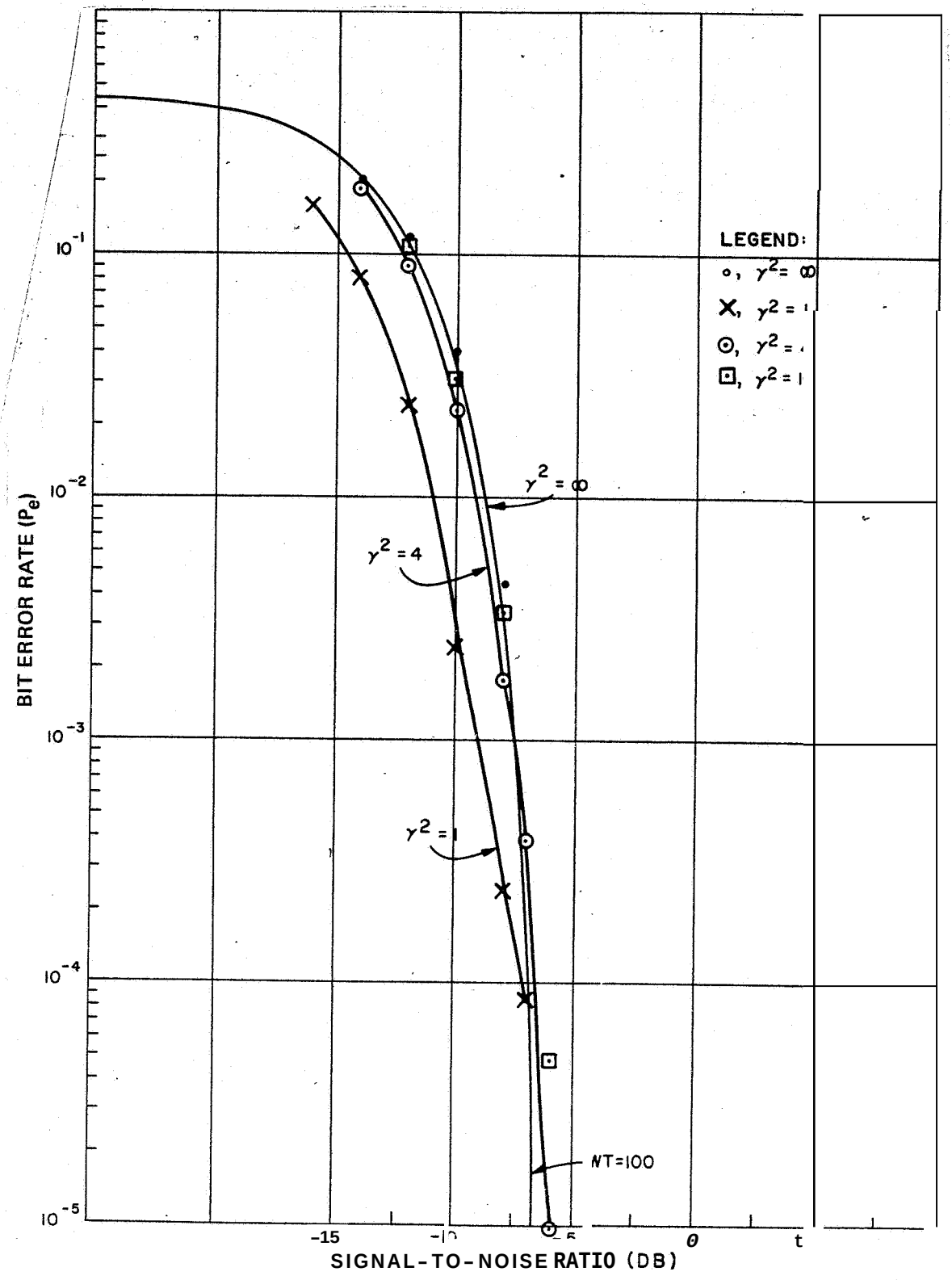

Figure III-10. Bit Error Rate as a Function of Signal-to-Noise Ratio and γ^2 for a Fading Bandwidth of I kHz (No Doppler Offset)

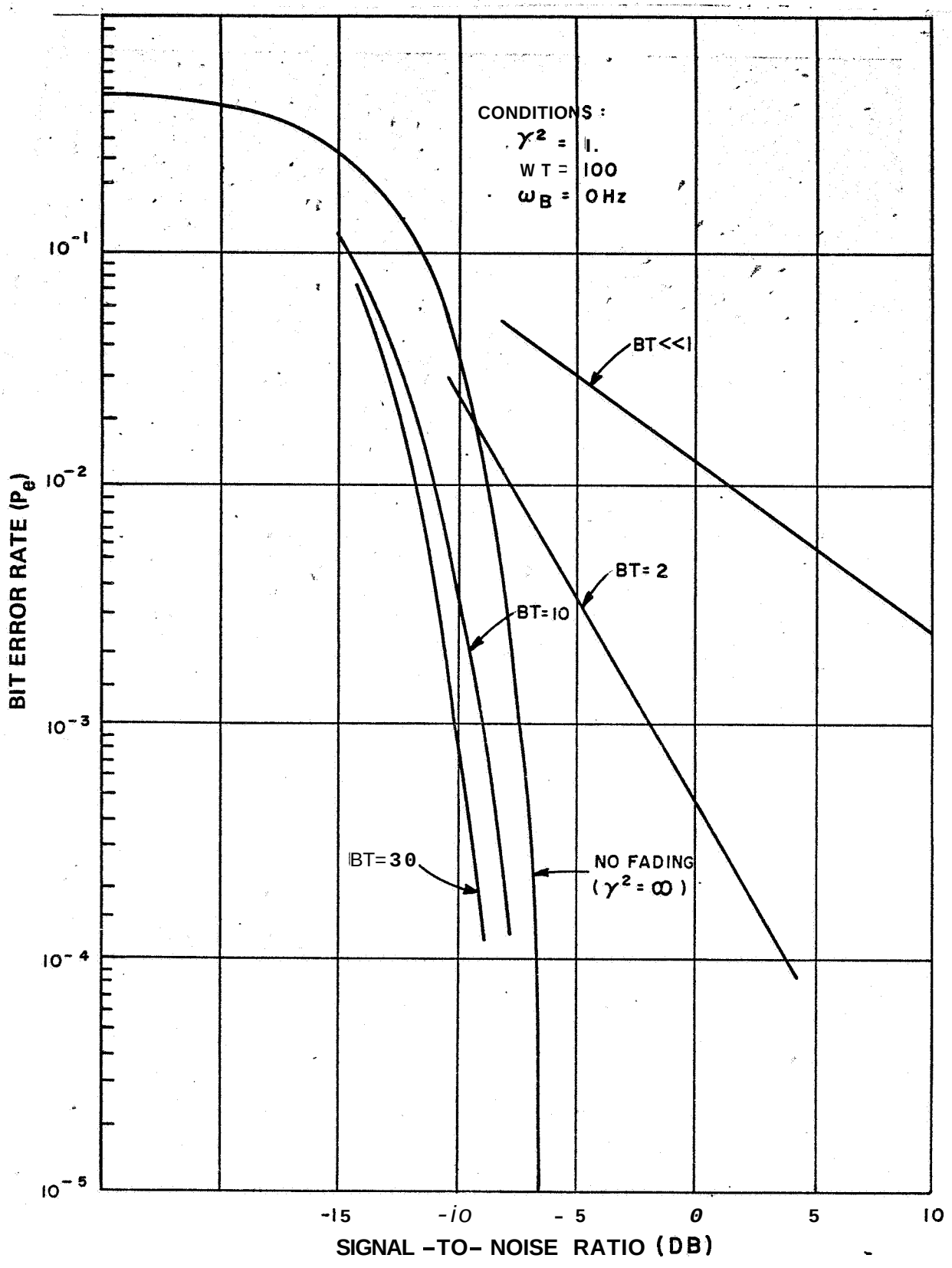

Figure III-11. Bit Error Rate as a Function of Direct Signal-to-Noise Ratio with Ratio of Fading Bandwidth to Data Rate (BT) as a Parameter

Figure III-12. Bit Error Rate as a Function of Signal–to–Noise Ratio and γ^2 for a Fading Bandwidth of 1 kHz and Bit Rate of 1 kHz (No Doppler Offset)

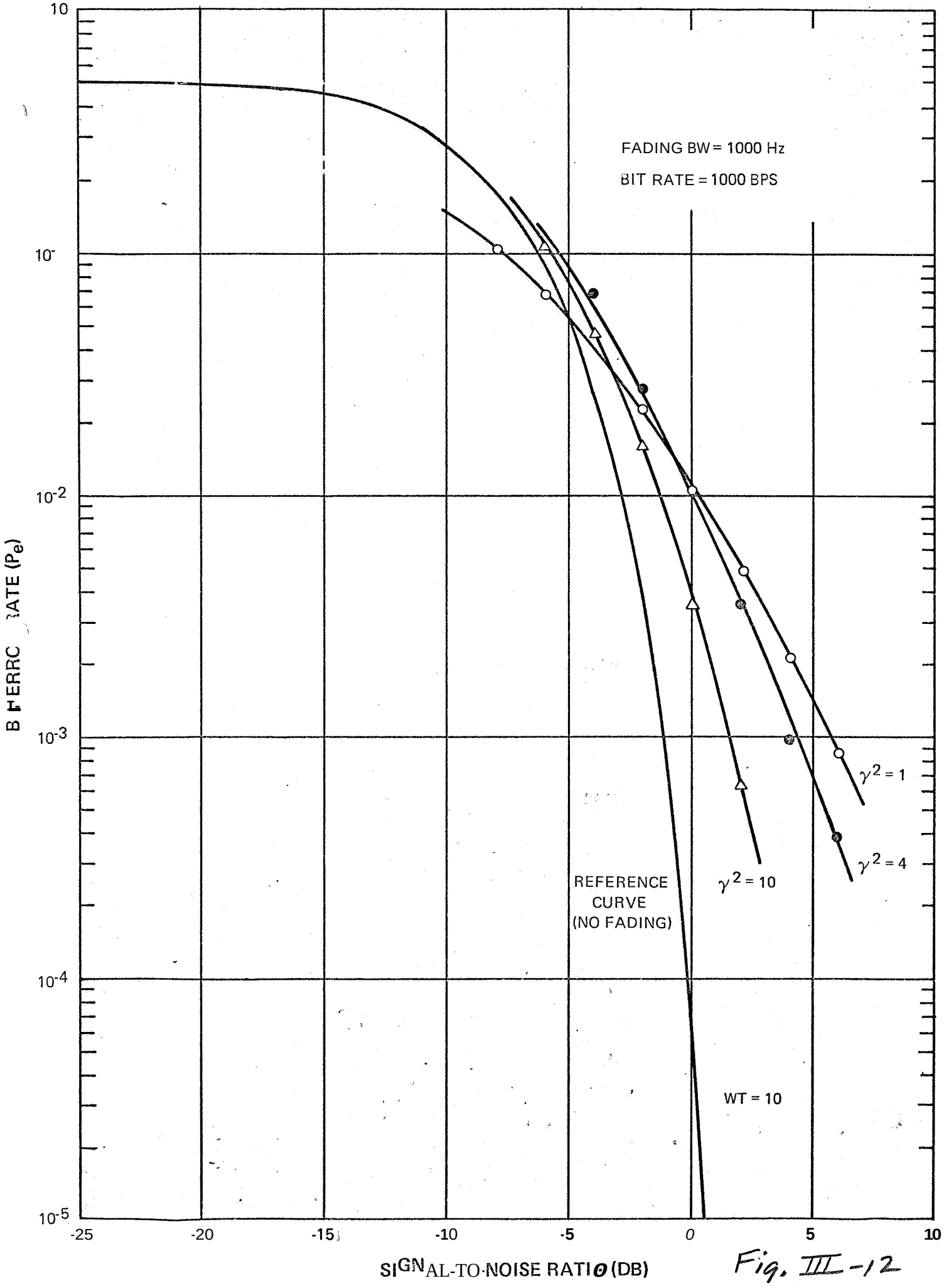
FADING BW = 1000 Hz
BIT RATE = 1000 BPS
$\gamma^2 = 1$
$\gamma^2 = 4$
$\gamma^2 = 10$
REFERENCE CURVE (NO FADING)
WT = 10
BIT ERROR RATE (P_e)
SIGNAL-TO-NOISE RATIO (DB)
10
10^{-1}
10^{-2}
10^{-3}
10^{-4}
10^{-5}
-25
-20
-15
-10
-5
0
5
10

Fig. III-12

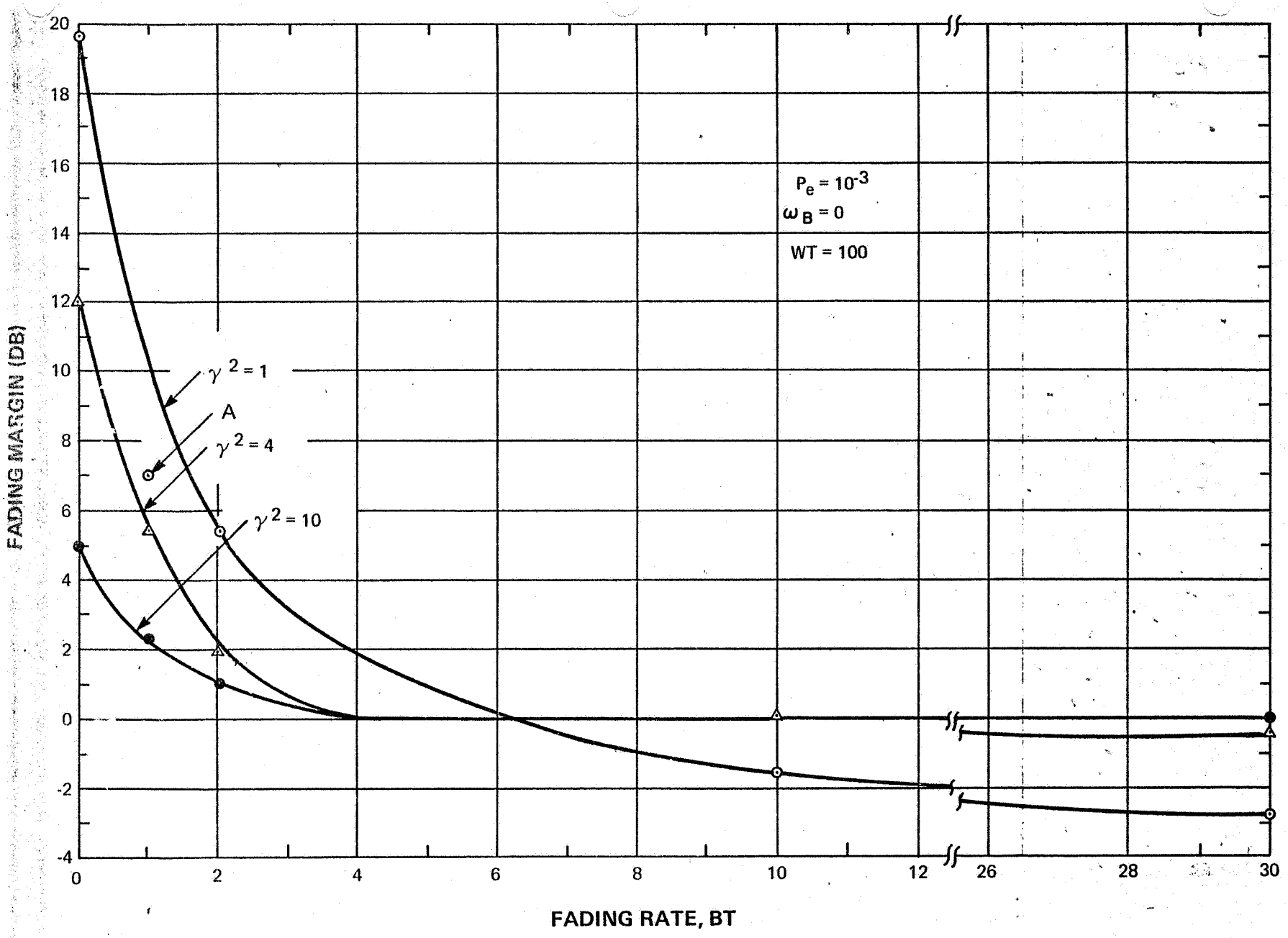

Figure III-13. Fading Margin as a Function of BT and γ^2 for WT = 100

which occurs at terminal velocity, is approximately **200 Hz** and corresponds to BT = **2** for the **100** bit-per-second data rate. **For** these considerations, a fading **margin** of **2** db would be required. If BT is greater **than 4** at $\gamma^2 = 4$, there would be **no** penalty introduced by planetary surface reflections. It should be pointed **out** here that Figure III-13 applies for a **WT = 100** and if this parameter is changed, a new set of curves would be required to determine the fading margin. It is for this reason that point **A** on Figure **111-13,** which was taken from the WT = 10 data (Figure **111-12)** for $\gamma^2 = 1$, BT = **1,** does not fit on the curve;

An interesting phenomena illustrated in Figure **111-13** is that for large BT products, the reflected signal aids the link performance. This is due to the fact that the FSK detector is basically an energy detector and if the reflected signal has zero correlation with the direct signal (Equation **111-21)** over the bit period, the detector will see the sum of the engeries {Equation **111-25).** The effect of rapidly varying scattering (fast fading) by a rough planetary surface is to convert the incident wave into noise-like reflected signal whose correlation with the direct signal decays rapidly with time.

c. Case **111:** Doppler Offset Larger Than Fading Bandwidth

In this case, $\omega_B >> B$ and, therefore,

$$B_1 \cos \omega_B t + B_2 \sin \omega_B t = Q \sin (\omega_B t + \Theta) \qquad \textbf{(In-27)}$$

where $Q = \sqrt{B_1^2 + B_2^2}$

and Θ can take on any value between 0 and 2π with equal likelihood.

Therefore, Equation 111-20 becomes

$$= \frac{1}{T}\int_0^T \left(1 + \frac{B_1}{A^2} + \frac{B_2^2}{A^2}\right) dt + \frac{2}{AT}\int_0^T Q \sin(\omega_B t + \Theta)\, dt \qquad \text{(III-28)}$$

'In.

When many cycles of ω_B are included in a bit period (T), then

$$\frac{2}{AT}\int_0^T B \sin(\omega_B t + \Theta)\, dt \to 0 \text{ as } \omega_B \to \infty \qquad \text{(In-29)}$$

Thus, for large $\omega_B t$ products ($\omega_B t \gg 1$):

$$\rho_{III} = \int_0^T \left(1 + \frac{B_1^2}{A^2} + \frac{B_2^2}{A^2}\right) dt \qquad \text{(III-30)}$$

ρ_{III} is always greater than unity, but is time varying as a function of $B_1 + B_2$.

The results of an experiment with fading bandwidth of 200 Hz and variable doppler offset for $\gamma^2 = 1$ are shown in Figure III-14. It can be seen that with no doppler offset and in the region of interest ($P_e = 10^{-3}$), the performance is degraded with respect to the no-multipath case. However, as doppler offset is introduced, the performance improves rapidly to the case where the performance with multipath is superior to that with no multipath Figure III-15 is a similar set of curves for a fading bandwidth of 1000 Hz. In this case, the fading bandwidth was such that even without doppler offset, the performance was superior to the no-miltipath case ($\gamma^2 = \infty$). The performance here improved with doppler offset to the limiting value predicted by

$$\rho_{II} = \frac{1}{T}\int_0^T \left(1 + \frac{B_1^2}{A^2} + \frac{B_2^2}{A^2}\right) dt = 1 + \frac{1}{\gamma^2} \qquad \text{(ID-31)}$$

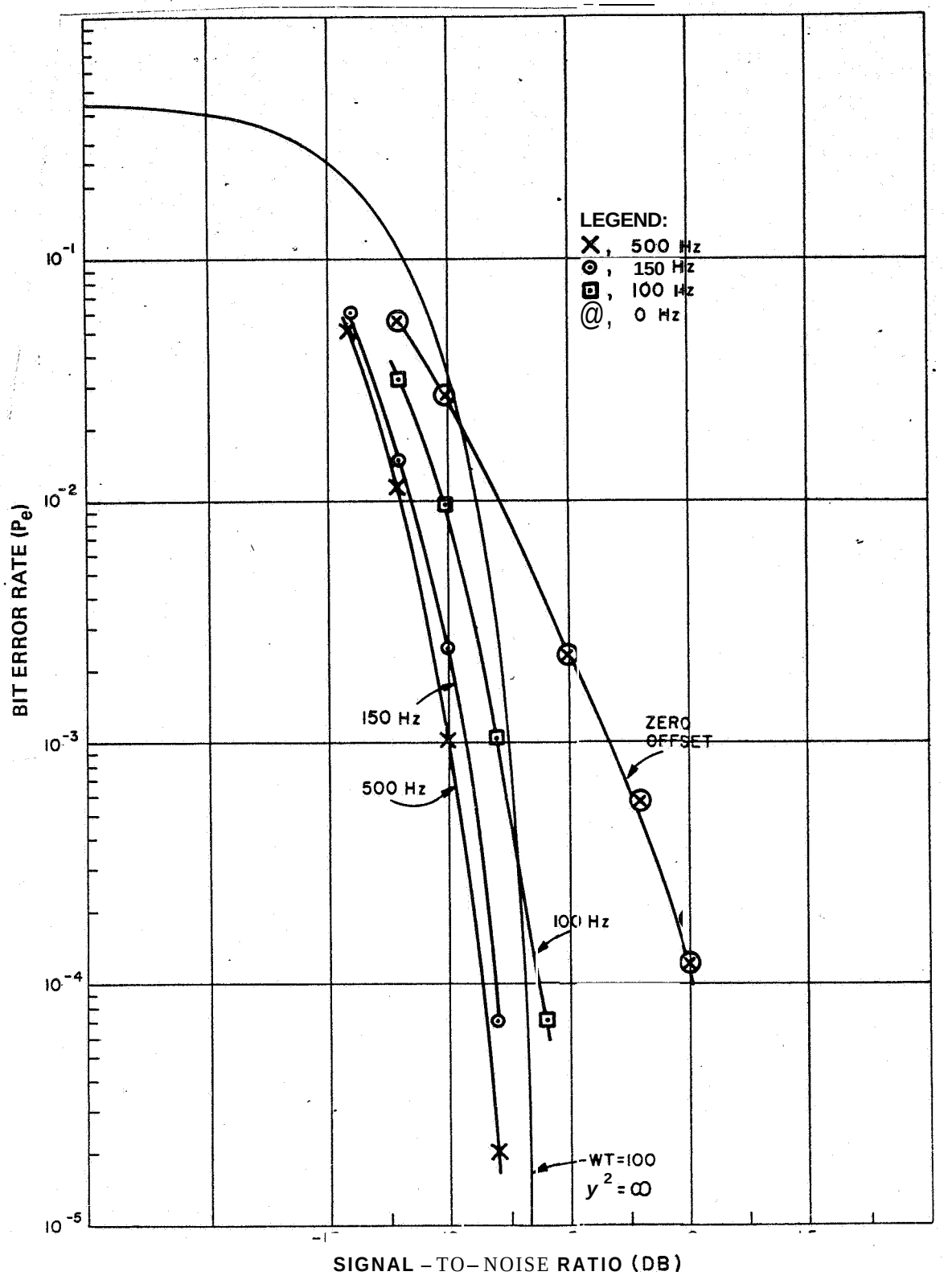

Figure III-14. Bit Error Rate as a Function of Signal-to-Noise Ratio **with** Variable Doppler Offset and a Fading Bandwidth of 200 Hz

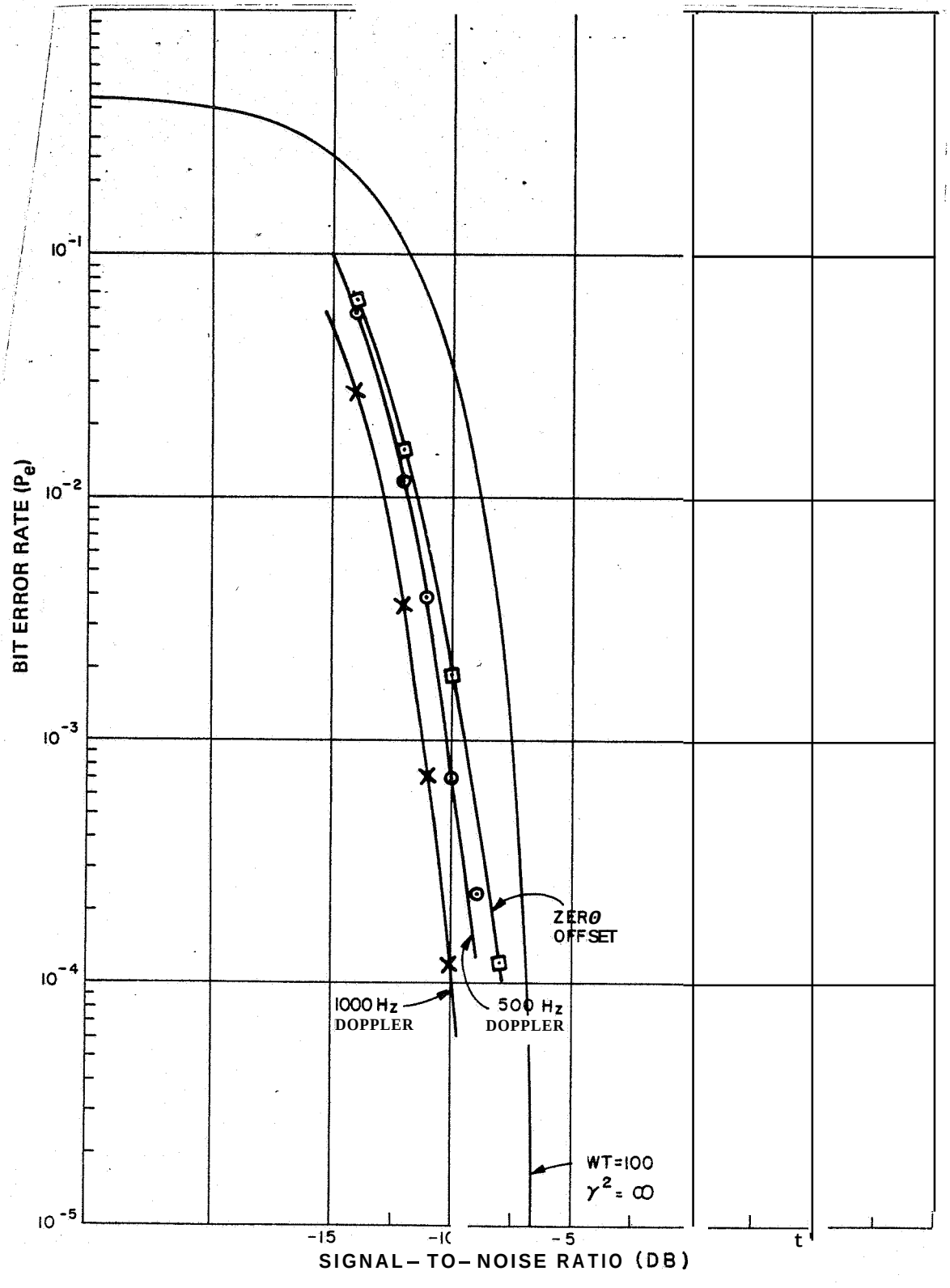

Figure III-15. Bit Error Rate as a Function of Signal–to–Noise Ratio with Variable Doppler Offset for Fading Bandwidth of 1 kHz

Since $\gamma^2 = 1$, the expected curve would be shifted 3 db to the left of the no-muitipath case. In this case, due to the high fading bandwidth,

$$\frac{1}{T}\int_0^T B_1^2 \rightarrow \overline{B_1^2}, \text{ and } \frac{1}{T}\int_0^T B_2^2 \rightarrow \overline{B_2^2} \qquad \text{(III-32)}$$

where $\overline{B_1^2} = \overline{R_s}$ is the power in the reflected signal.

d. Case IV: Moderate Fading Bandwidth, Moderate Doppler Offset

Figure III-16 shows a set of data for a 200-Hz fading bandwidth with 3-kHz doppler offset and variable γ^2. The doppler offset is sufficiently great so that the performance is always better than for no multipath. However, the curves are not displaced by a constant $1+\frac{1}{\gamma^2}$ as would be the case for a higher fading bandwidth. The 1000-Hz offset curve for 1000-Hz fading bandwidth of Figure 111-15 does show a nearly constant offset. Even for a 3000-Hz fading bandwidth with no doppler offset (Figure 111-8), the curves are not as parallel as for the 1000-Hz offset, 1000-Hz fading bandwidth curves of Figure 111-15. Equation 111-8 shows that for sufficiently large fading bandwidth, the curves will be parallel without doppler offset. However, this ideal can be approached more rapidly by introducing some doppler offset. Therefore, the most desirable situation is to have a combination of fading bandwidth and doppler offset. For example, the data shows (Figure III-14) for a fading bandwidth of 200 Hz, and a doppler offset of 200 Hz (the estimated terminal impact values), there would be performance improvement at the design center of $P_e = 10^{-3}$. This applies to a bit rate of 100 bits per second; however, the conclusion can be generalized by referring to frequency time products.

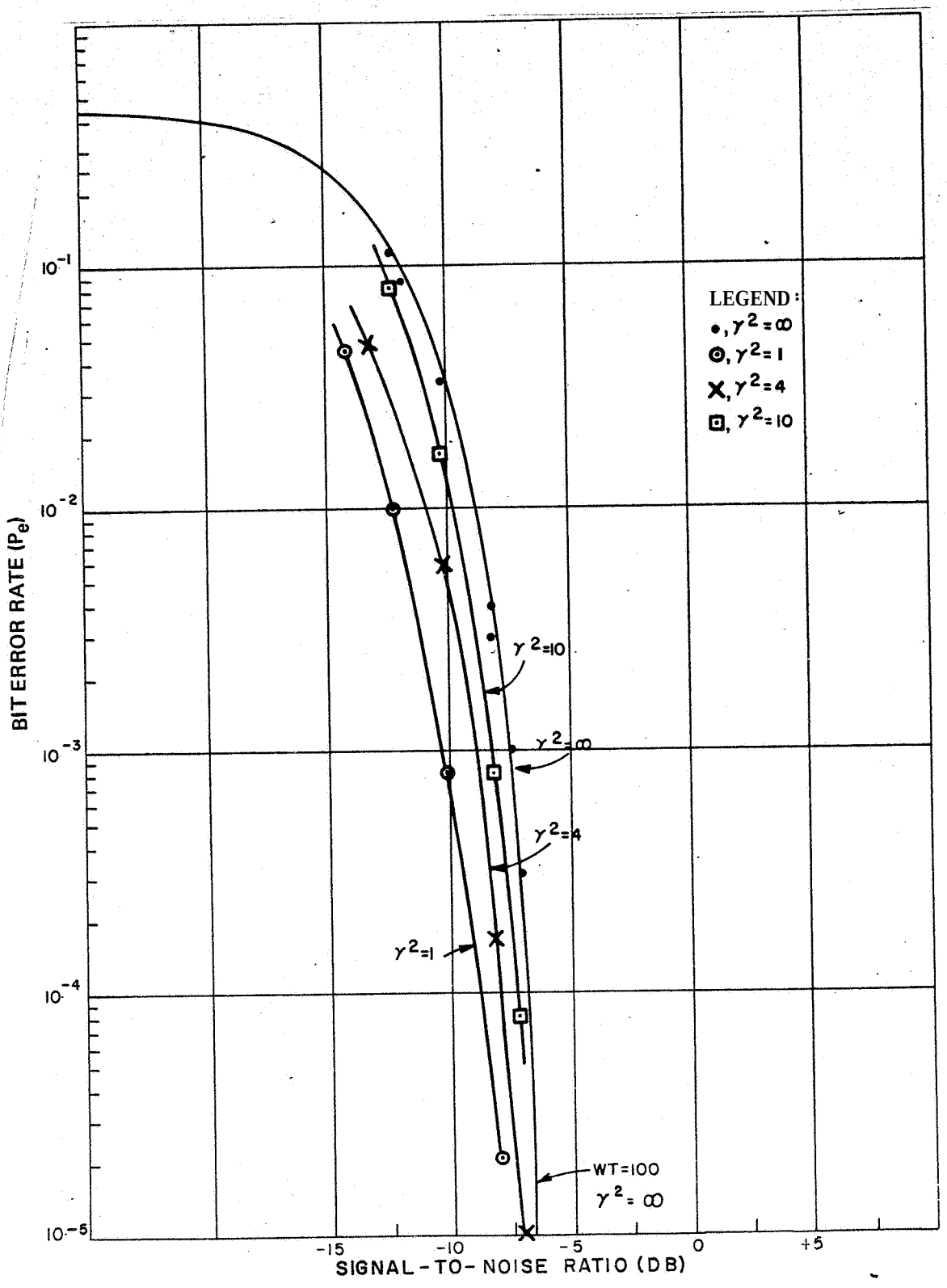

Figure III-16. Bit Error Rate as a Function of Signal-to-Noise Ratio with Variable γ^2 and a Fading Bandwidth of 200 Hz and a Doppler Offset of 3 kHz

Therefore, in general terms, if

BT (fading bandwidth X bit period) >2

and $\omega_B T$ (offset frequency X bit period) >2

there will be no degradation of performance due to multipath and in fact, there will be some improvement depending on γ^2. The exact shape of the performance curves is determined also by the WT parameter and therefore, the numerical values presented apply only for WT = 100. However, the general conclusion still applies that the most effective mechanism to reduce the adverse effect of multipath is to have moderate fading bandwidth with some doppler offset.

Thus for the phenomena of link performance improvement due to multipath has been discussed. The purpose of the study was to determine the effect of a possible multipath environment to ensure the success of the link. At our present state of knowledge, we cannot guarantee a very specific set of surface characteristics in order to define the multipath environment precisely. The best that can be done with the limited knowledge available is to postulate a set of typical-case conditions to ensure adequacy of the link in the event that surface reflections are present but in no way count on them to be present to aid the link performance. Thus, multipath becomes a possible degradation factor but should not be used to aid link performance.

D. REFERENCES

1. Selected Studies of VHF/UHF Communications for Planetary (Mars/Venus) Relay Links, Final Report, Contract No. NAS2-3772, issued January 15, 1967.

2. Reference Data for Radio Engineers, ITT Corporation, Fourth Edition, page 991,

3. Communication Systems and Techniques, Schwartz, Bennett, and Stein, McGraw-Hill, 1966, Page 25.

4. Information Transmission, Modulation, and Noise, Schwartz, McGraw-Hill, 1959, Sections 7-9.

SECTIONIV

EFFECT OF A BIT SYNCHRONIZER ON LINK PERFORMANCE (TASK 4)

A. INTRODUCTION AND SUMMARY

The previous study' experimentally evaluated the effects of slow fading ($BT << 1$) on the performance of the link with a bit synchronizer. The purpose of this experiment is to determine the effects of fast fading ($BT \geq 2$), with and without doppler offset, on the performance of the link with a bit synchronizer. In the tests, the FSK receiver was operated with bit synchronization derived from the data signal, as contrasted to Task 3 (Section III) where the bit synchronization was hardwire-connected from the data source.

The results of the earlier study showed a degradation of the order of 2 db at error rates of 10^{-3} due to use of the bit synchronizer in the presence of slow fading ($\gamma^2 = 4$ and $\gamma^2 = 10$). The degradation was even greater for larger error rates. The results of the fast-fading experiment showed no degradation due to the fading. A uniform degradation of the order of 0.5 db was introduced by the bit synchronizer; however, this degradation was noted whether or not there was fading present.

B. EXPERIMENT IMPLEMENTATION

The equipment used for this experiment is identical to that employeh in the slow-fading tests and is described in Reference 1, Section 5.2. The bit syn-

chronizer employed was a Telemetrics Model 6203A. The tests were conducted on "A", "B" comparison basis where at each signal–to–noise ratio, the bit error rate was first measured with hardwire sync and then measured with the bit synchronizer in place of the hardwire sync.

C. EXPERIMENTAL RESULTS

The effect of the bit synchronizer was first measured in the absence of fading ($\gamma^2 = \infty$). The data are presented in Figure IV–I. The measured data points are shown plotted along with the theoretical (perfect sync) curve. The data show a small degradation, on the order of 0.5 db, for error rates between 10^{-2} and 10^{-3}. These results are consistent with those obtained in the previous study.

The fast–fading tests were performed under conditions corresponding to three points in the sample mission, i.e.:

Fading bandwidth = 3,000 Hz Doppler offset = 3,000 Hz	(Just emerging from blackout)
Fading bandwidth = 1,000 Hz Doppler offset = 1,000 Hz	(Intermediate between blackout and terminal impact)
Fading bandwidth = 200 Hz Doppler offset = 500 Hz	(Just prior to impact)

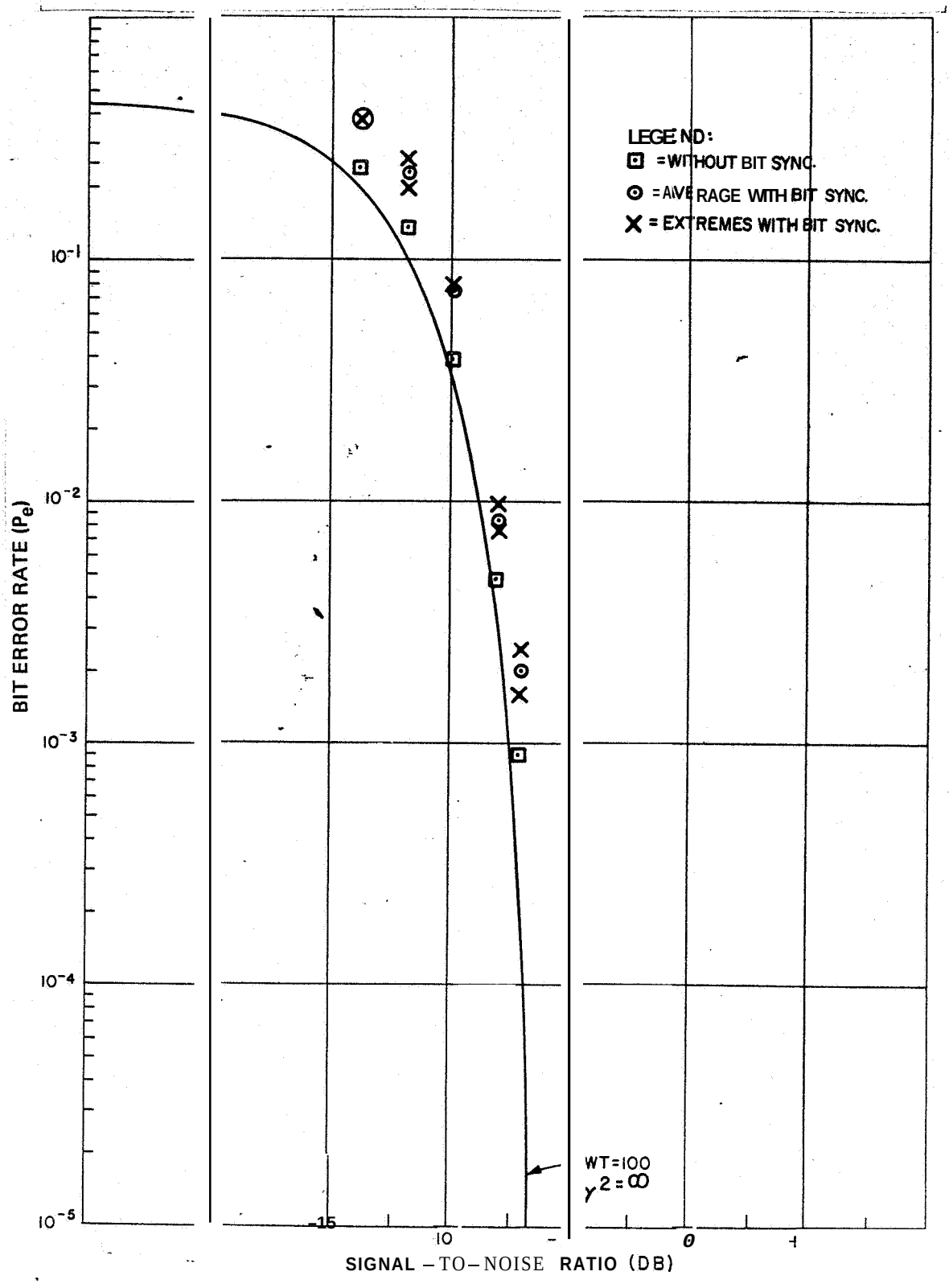

Figure IV-1. Bit Error Rate as a Function of Signal–to–Noise Ratio with No Fading. Showing the Effects of a Bit Synchronizer

The results of these tests are shown in Figures IV-2, IV-3, and IV-4. The data show consistent displacement of the bit synchronizer curves of about 0.5 db; however, within the limits of experimental accuracy this degradation is no more than that observed without multipath.

The effect of using a bit synchronizer in the presence of slow fading is shown in Figure IV-5 to illustrate the pronounced impact of slow fading on link performance. In the case of very slow fading, fades occur of sufficient time duration to cause loss of lock in the bit synchronizer. The reacquisition process then introduces a loss of data beyond that caused by the fading itself, thus in effect, increasing the error rate. For the case investigated here, 200-Hz fading bandwidth and greater, the probability of a fade being of sufficient duration to cause loss of lock is extremely small and therefore, the results obtained are not unexpected. These results are further substantiated by the findings of Task 6 (see Section V) which show that even for 200-Hz fading bandwidth without doppler offset, there is no discernable correlation between bit errors, or in other words, given that an error occurs, the probability that succeeding bits will be in error is not affected. This means there is no clustering of errors and the probability of a synchronizer loop dropout is small.

The conclusion then, is, that the use of a bit synchronizer in the presence of fast fading does not cause system error rate performance degradation beyond that caused by the bit synchronizer in the absence of fading.

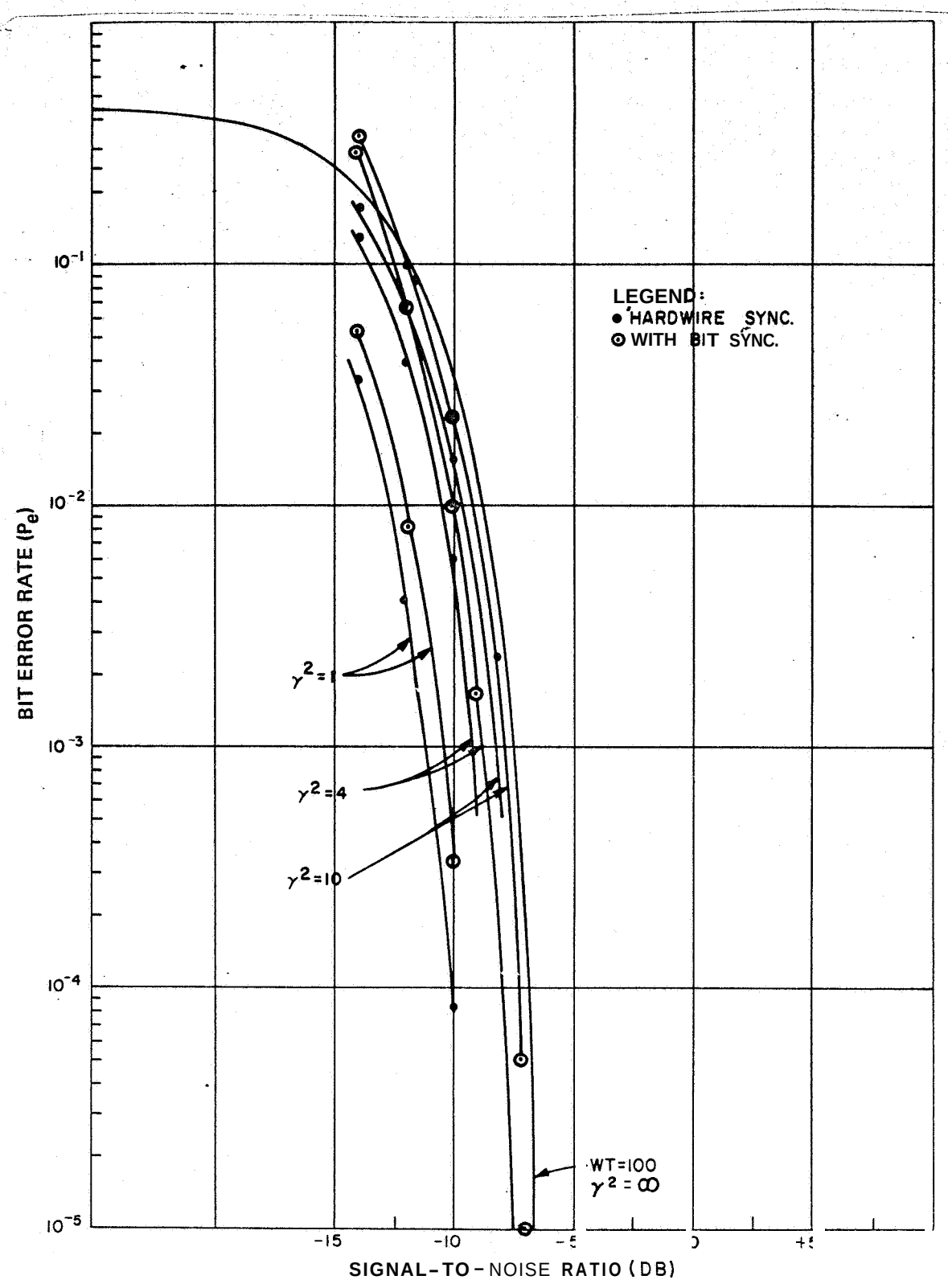

Figure **IV-2.** Effect of a Bit Synchronizer on Bit Error Rate for a Fading Bandwidth of **3** kHz and a Doppler Offset of **3** kHz, γ^2 Variable

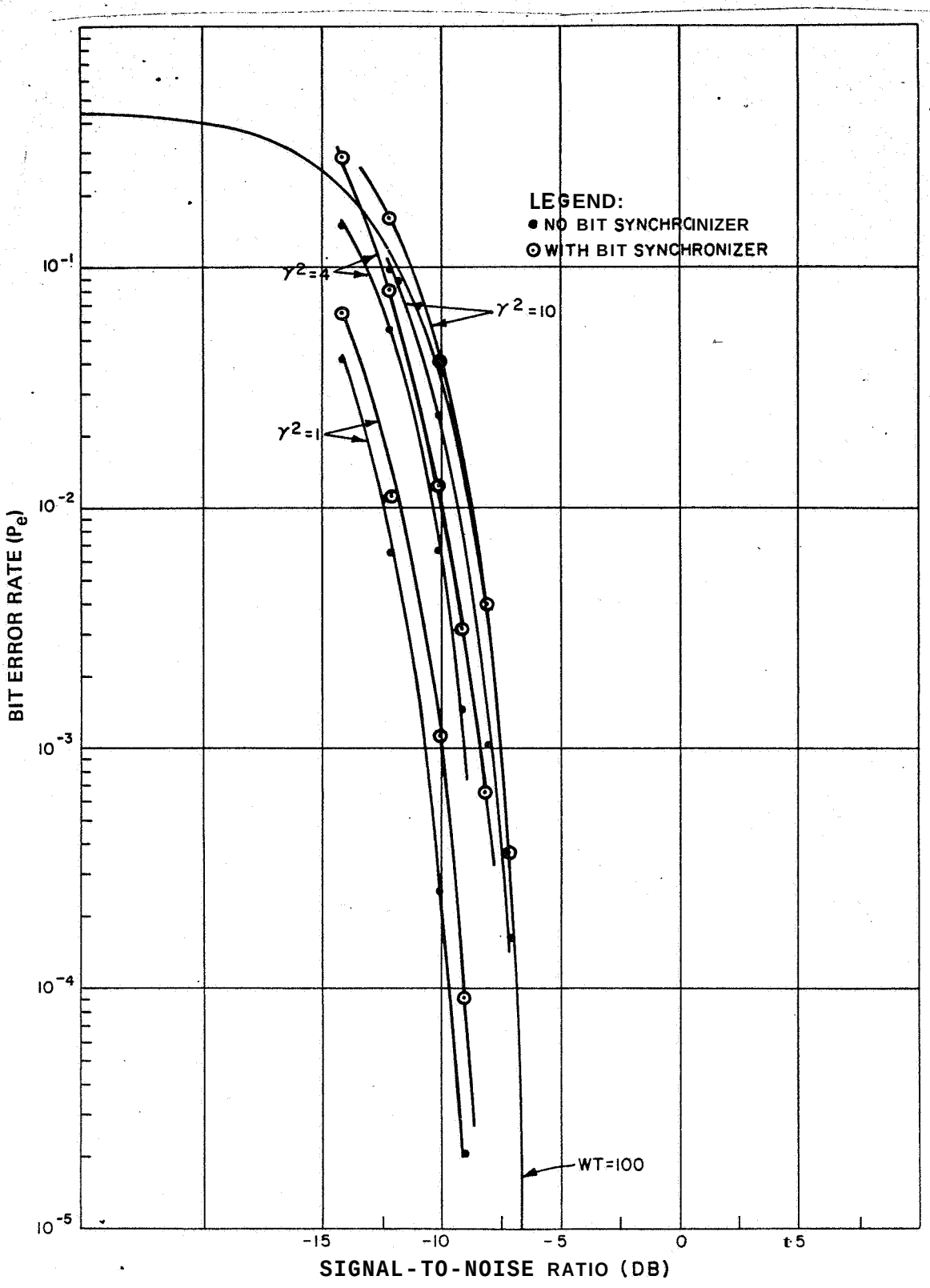

Figure IV-3. Effect of a Bit Synchronizer on Bit Error Rate for a Fading Bandwidth of 1kHz and a Doppler Offset of 1 kHz, γ^2 Variable

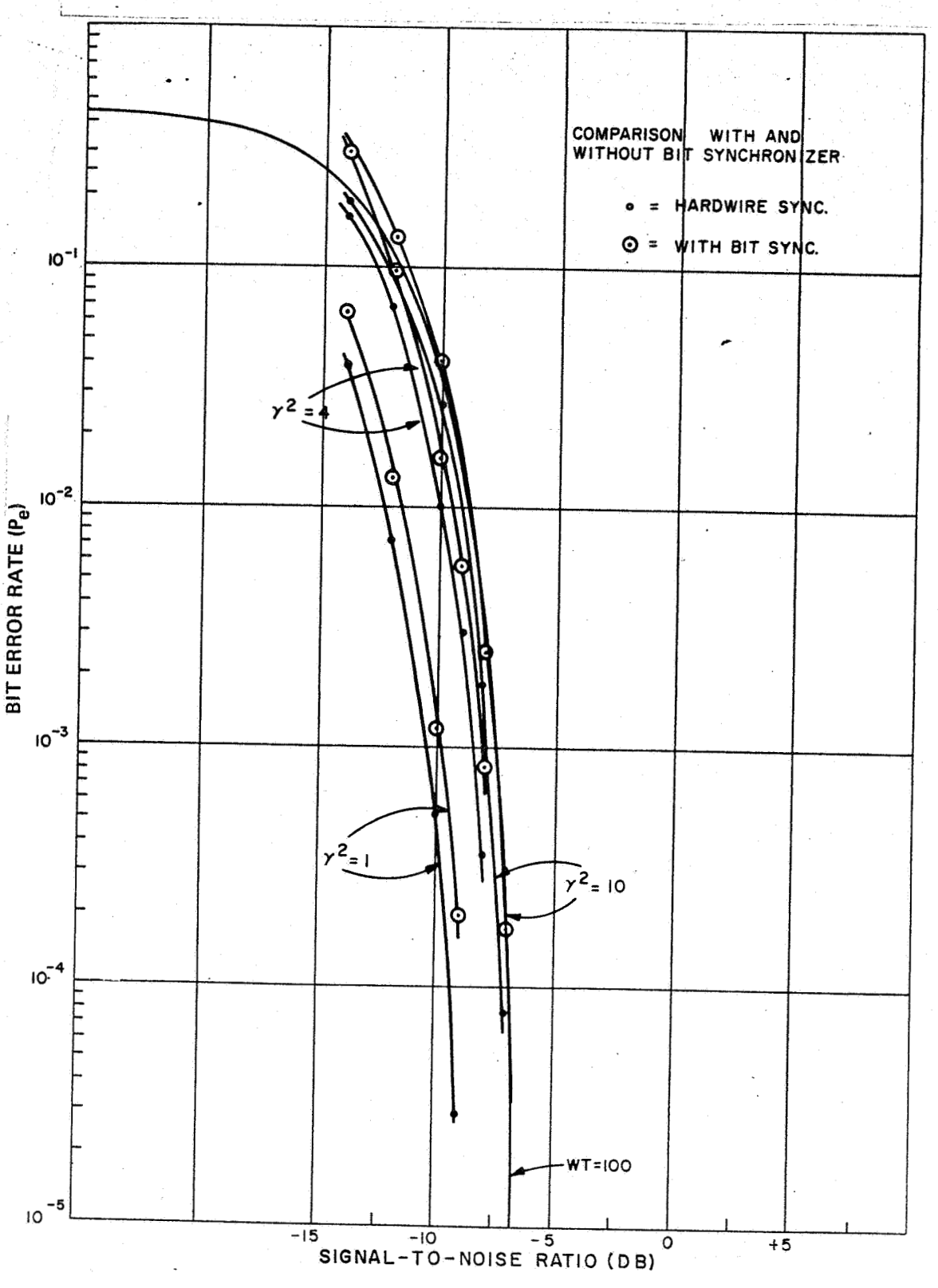

Figure IV-4. Effect of a Bit Synchronizer on Bit Error Rate for a Fading Bandwidth of 200 kHz and a Doppler Offset of 500 Hz, γ^2 Variable

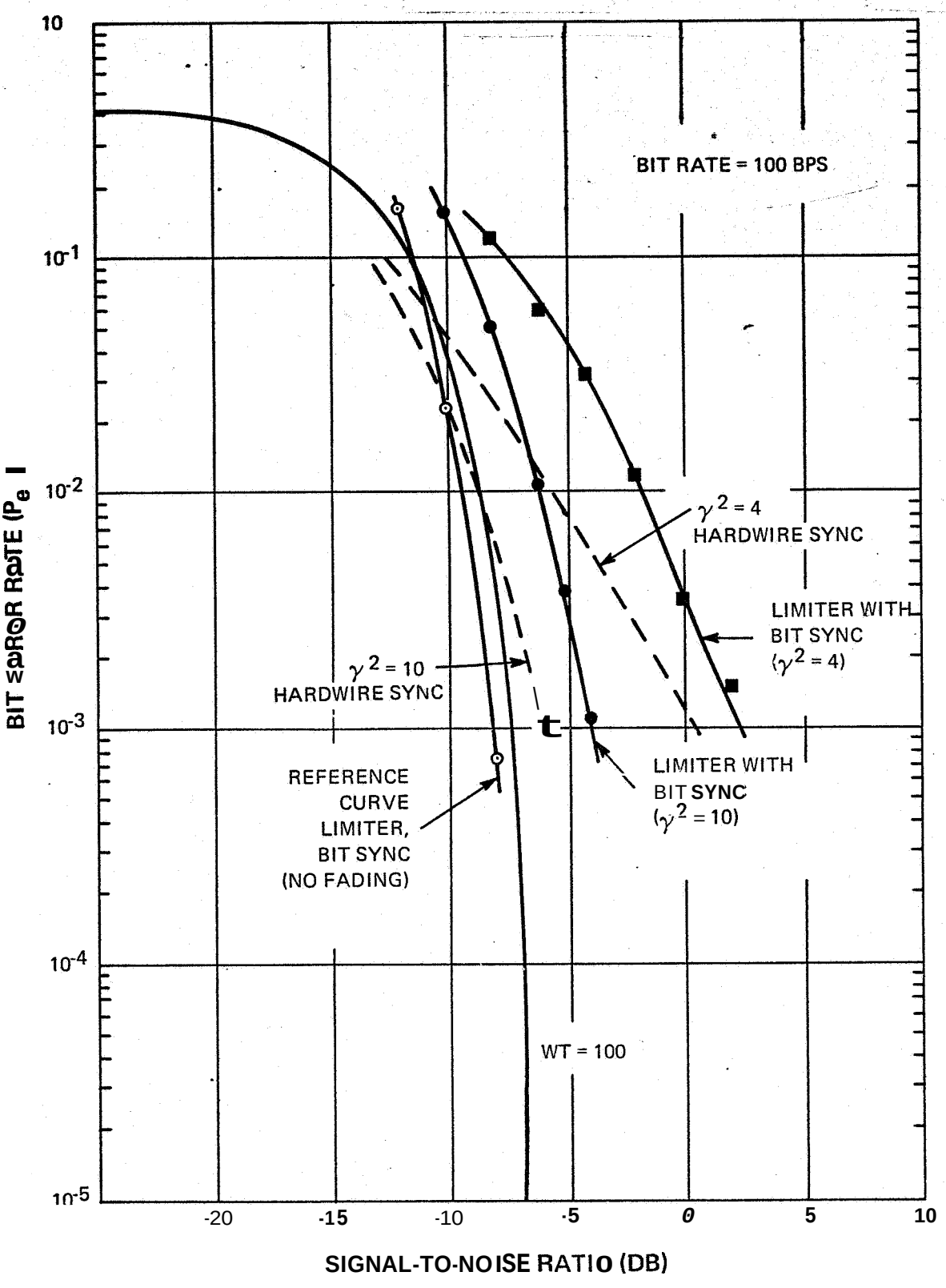

Figure **N-5.** Effec" of a Bit Synchronizer for Very Slow Fading (BT << 1)

D. REFERENCES

1. Selected Studies of VHF/UHF Communications for Planetary (Mars/Venus) Relay Links, Final Report, Contract NAS 2-3772, issued January 15, 1967.

SECTION V

LINK PERFORMANCE CRITERLA (TASK 6)

A. INTRODUCTION AND SUMMARY

The performance of digital transmission systems is most often specified in terms of bit error rate. The assumption implicit in such a performance criteria is that the errors are random and independent. This means that the probability of an error for any given data bit is the same as for any other bit and that past errors and future errors do not influence the probability of error. In communications systems that operate under conditions where white Gaussian noise is added to a fixed signal, the occurrence of bit errors is random and independent. In a multipath environment, the signal amplitude is not fixed, but varies in some random manner before the addition of the Gaussian receiver noise. Where multipath causes slow fading (fading period is greater than a bit period), deep fades occur which result in a high error rate over the duration of the fade. Since the fading period is greater than the bit period, the probability of error is not independent from bit to bit. System performance in such cases is often specified in the percentage of time the system operates with a low error rate. An example of this is the use of percentiles for expressing the perfcrmance of troposcatter systems.

The experiment performed here is to determine whether the FSK system produces random, independent errors under the expected conditions of fast fading. The system was tested over a range of fading bandwidths and doppler offsets for

small sample lengths (700 bits) and the error distribution compared to that predicted by theory, assuming random independent errors. The results showed good correspondence between prediction and measurement indicating that the errors are truly independent and random. The conclusion is that for the range of parameters investigated ($BT > 2$ and $\gamma^2 > 1$), the average bit error rate is a valid measure of performance.

B. EXPERIMENT IMPLEMENTATION

The equipment used for this experiment was the same as that employed for implementing the experiment of Task 4. The error counter was programmed to read the number of errors in a 700- or 1400-bit sample rather than a 10,000- or 100,000-bit sample. In Task 4 (Section IV), the objective was to obtain the average error rate; therefore, very long sample lengths were necessary to ensure a sufficient number of errors in the sample to provide a high confidence that the average had been approached. The purpose of this task is to observe the errors in many small samples to determine the distribution of the errors among the samples.

C. EXPERIMENTAL RESULTS

The probability of K errors occurring in a sample of η bits for independent, randomly occurring errors is given by:

$$P_K = C_K^{\eta} (P_e)^K (Q_e)^{(\eta - K)} \qquad \text{(V-1)}$$

where

P_K is the probability of K errors;

C_K^{η} is the combination of η things taken K at a time;

P_e is the probability of a bit error; **and**

Q_e is the probability of no error = $(1-P_e)$.

Equation V-1 is the binomial distribution which can be written as

$$P_K = \frac{\eta!\ (P_e)^K\ (1-P_e)^{(\eta\ -K)}}{K\ !\ (\eta\ -K)\ !} \qquad \text{(V-2)}$$

The average or expected value of K is ηP_e and the variance is $\eta P_e(1-P_e)$. When η is large compared to K ($\eta >> K$) and P_e is small compared to unity, the binomial distribution is approximated by the Poisson distribution,

$$P_K = \frac{(\eta\ P_e)^K\ e^{-\eta\ P_e}}{K!} \qquad \text{(V-3)}$$

In the present experiment, the Poisson distribution was used because the approximation is very good since P_e is on the order of 10^{-3} and K is less than 10 compared to an η of 700. For the case $P_e << 1$, the expected value and variance of the binomial distribution is the same as that for the Poisson distribution.

From the experimental data, the total number of bits and total number of errors were calculated and the probability of error for each run was computed by

$$P_e = \frac{n_e}{N\eta} \qquad \text{(V-4)}$$

where

n_e is the total number of errors;

N is the number of samples (approximately 100 samples per run); and

η is the number of bits per sample.

This then gave the average probability of error for the overall run, The measured P_e was used in the Poisson equation to predict the error distribution. The number of samples containing K errors was then plotted as a function of K to give an error-density distribution. The predicted values were then compared to the measured values in graphical format.

The tests were performed over a range of conditions similar to that which would be experienced during a typical mission profile. The intention was to perform the tests at a signal-to-noise ratio corresponding to a bit error rate of 10^{-3}. The mean bit error rate is a calculated value from a run of data. In order to approach the desired bit error rate, a lengthy reiterative procedure is required (approximately 30 minutes per iteration or run). The bit error rate is quite sensitive to small changes in input signal-to-noise ratio which is variable in one-db steps. In most cases, a one-db change in signal-to-noise ratio produces an order of magnitude change in bit error rate in the vicinity of interest.

(The experimental curves of Task 3, for fast fading, demonstrate this characteristic.) Therefore, although the objective was to perform the tests at $P_e = 10^{-3}$, the actual values of P_e varied from 5×10^{-4} to 2×10^{-3}. This includes the effect of equipment stability, which is minor, during the runs.

The first two runs were performed with no fading; one for a sample length of 700 bits and one for a sample length of 1400 bits. The results are presented in Figures V-1 and V-2. The measured distribution of errors is in close agreement with the predicted distributions for independent, randomly occurring errors. This is expected for the non-fading case and indicated that the experimental set-up is operating satisfactorily.

The next series of runs was performed under fast-fading conditions simulating three phases of the probe descending through the planetary atmosphere as follows:

Phase I - Just After Emerging from Blackout.

B = 3000 Hz	$\gamma^2 = 10$	Figure V-3
ω_B = 3000 Hz	$\gamma^2 = 4$	Figure V-4

Phase II - Midway in the Mission.

B = 100 Hz	γ^2 10	Figure V-5
ω_B = 1000 Hz	$\gamma^2 = 4$	Figure V-6

Phase III - Just Before Terminal Impact.

B = 200 Hz	$\gamma^2 = 10$	Figure V-7
ω_B = 500 Hz	$\gamma^2 = 4$	Figure V-8

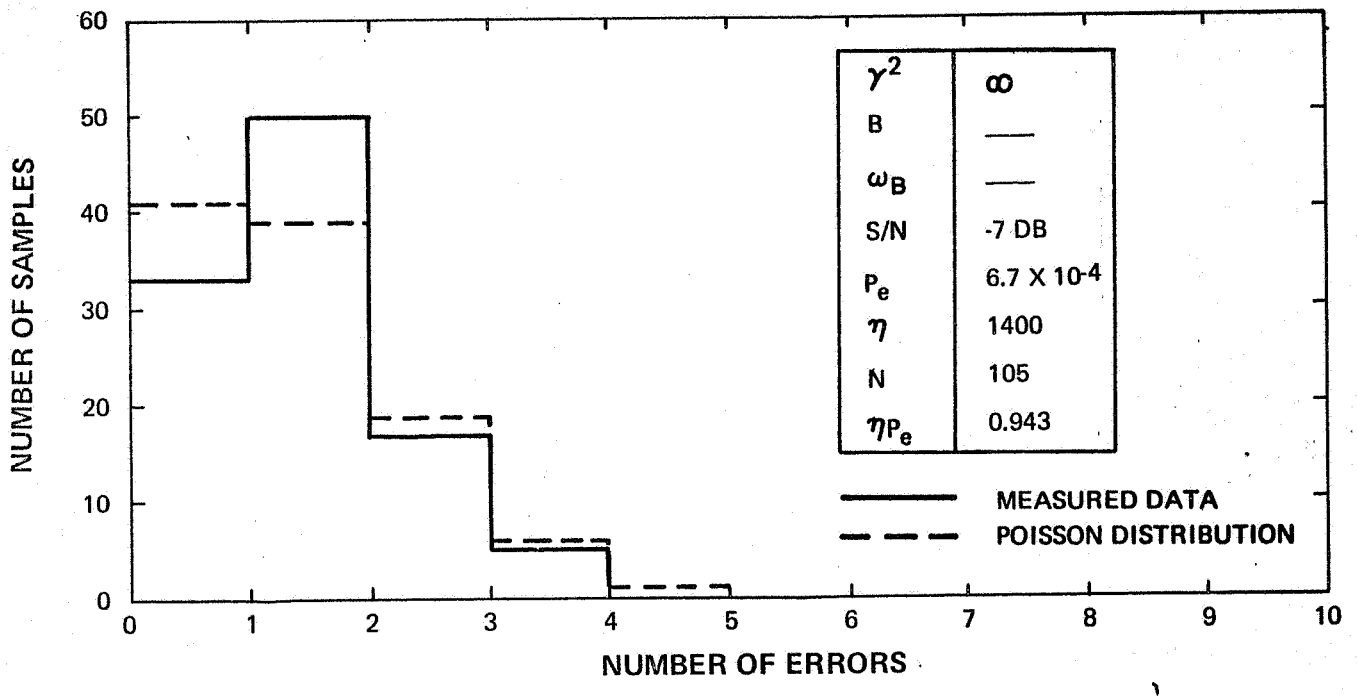

Figure V-1. Error Distribution with No Fading, 1400-Bit Sample

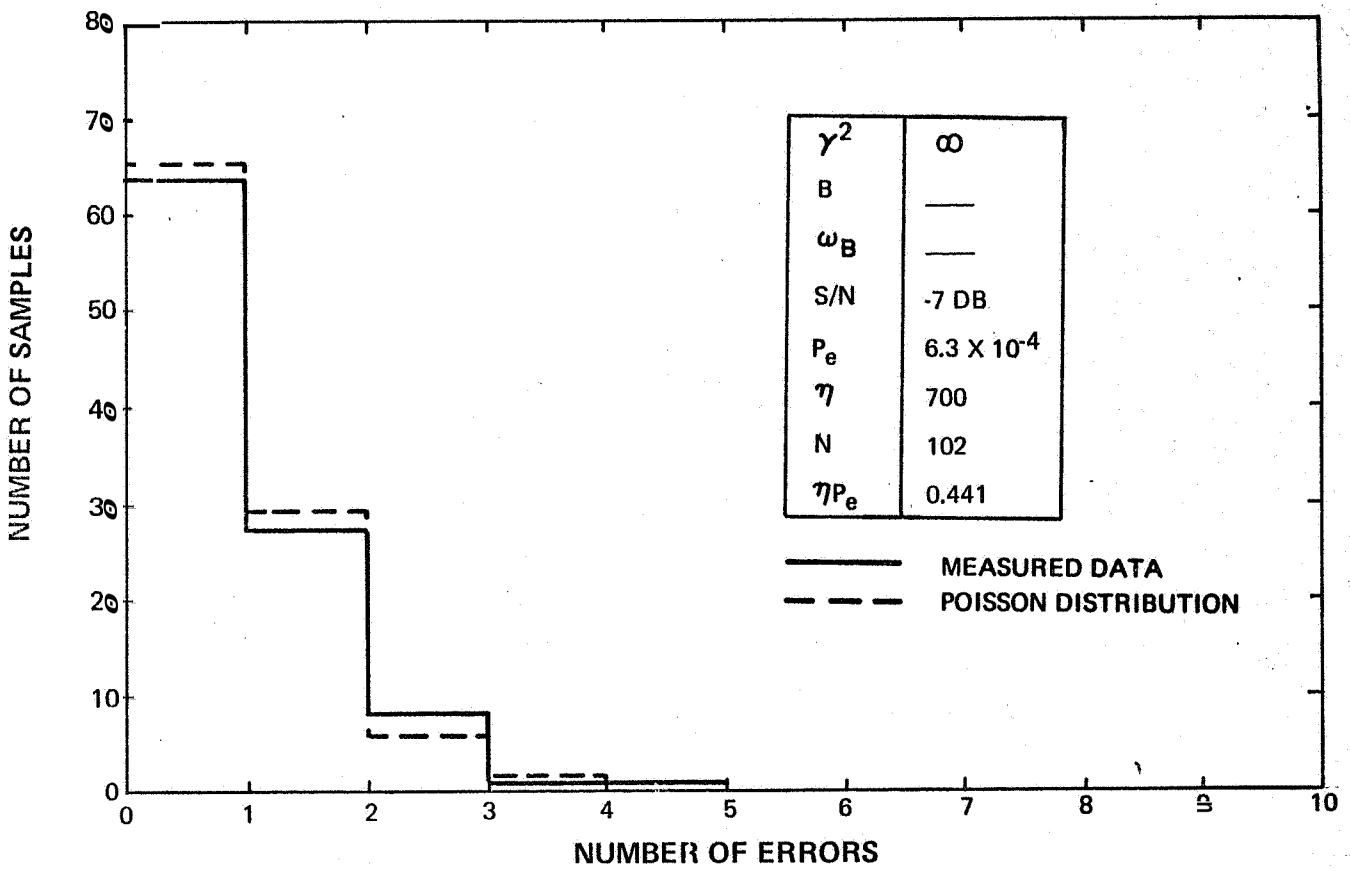

Figure V-2. Error Distribution with No Fading, 700-Bit Sample

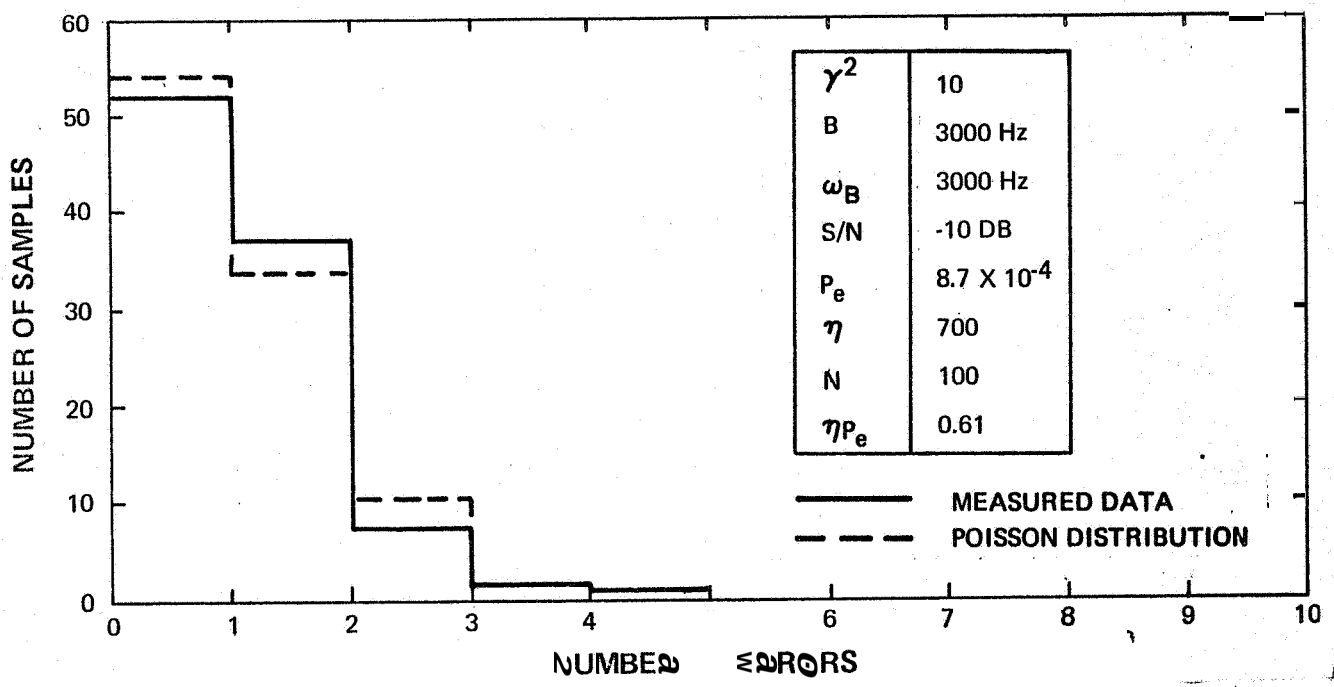

Figure V-3 Error Distribution for B = 3000 Hz, ω_B = 3000 Hz with $\gamma^2 = 10$

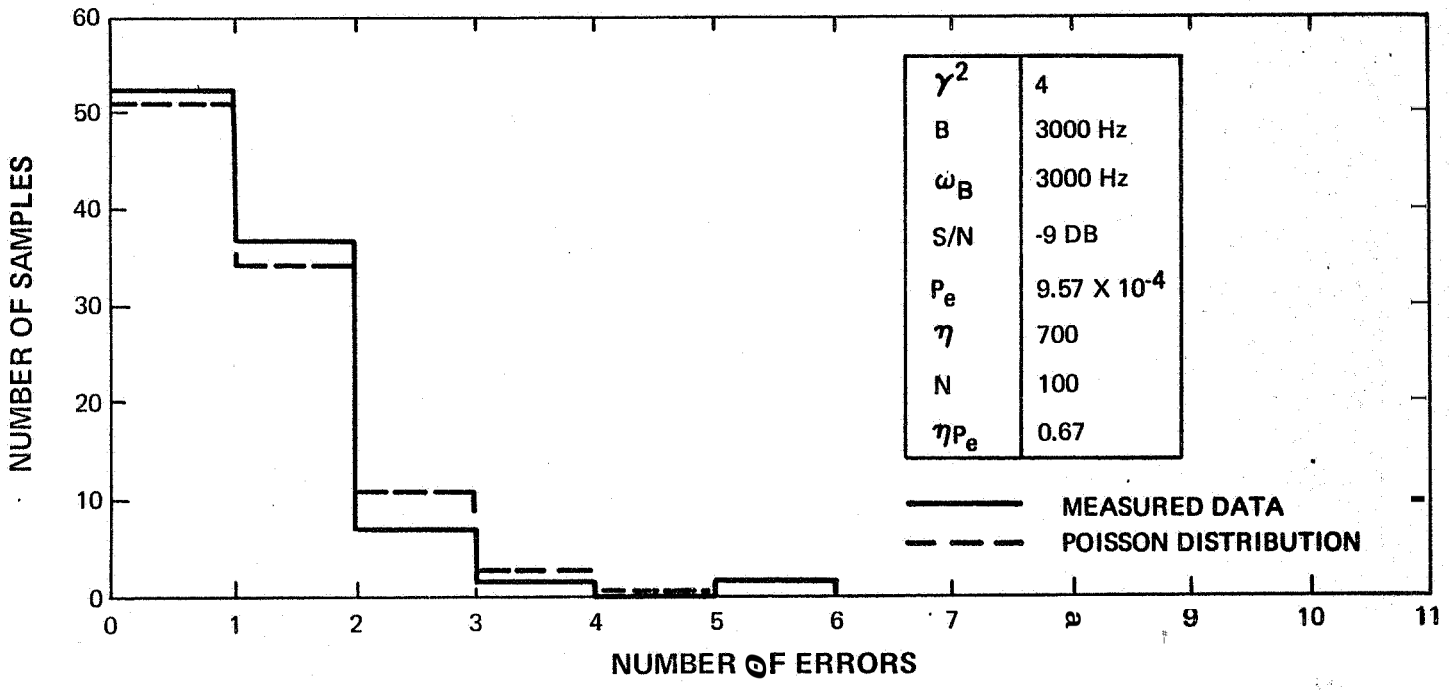

Figure V-4. Error Distribution for B = 3000 Hz, ω_B = 3000 Hz with $\gamma^2 = 4$

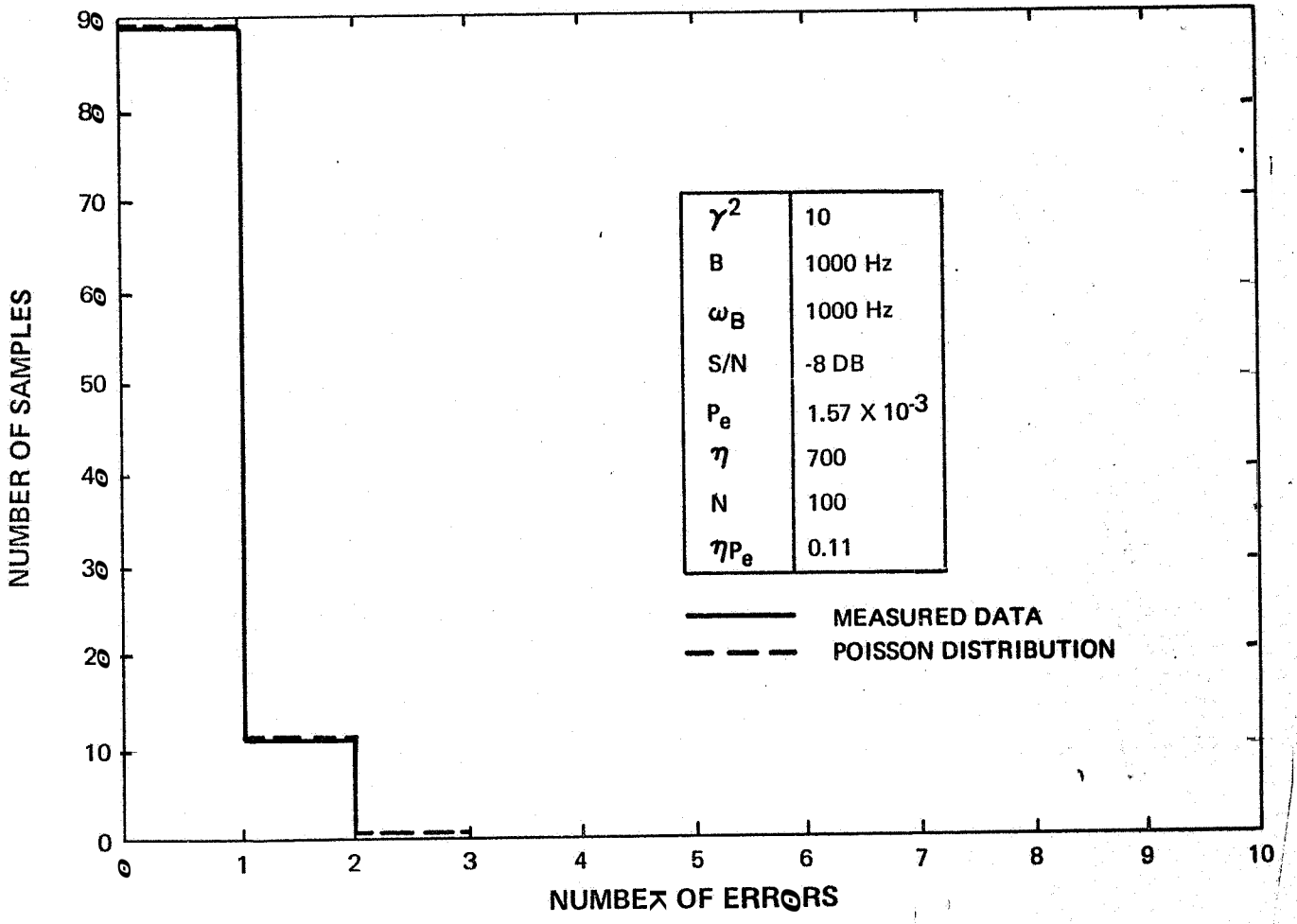

Figure V-5. Error Distribution for B = 1000 Hz, ω_B = 1000 Hz with $\gamma^2 = 10$

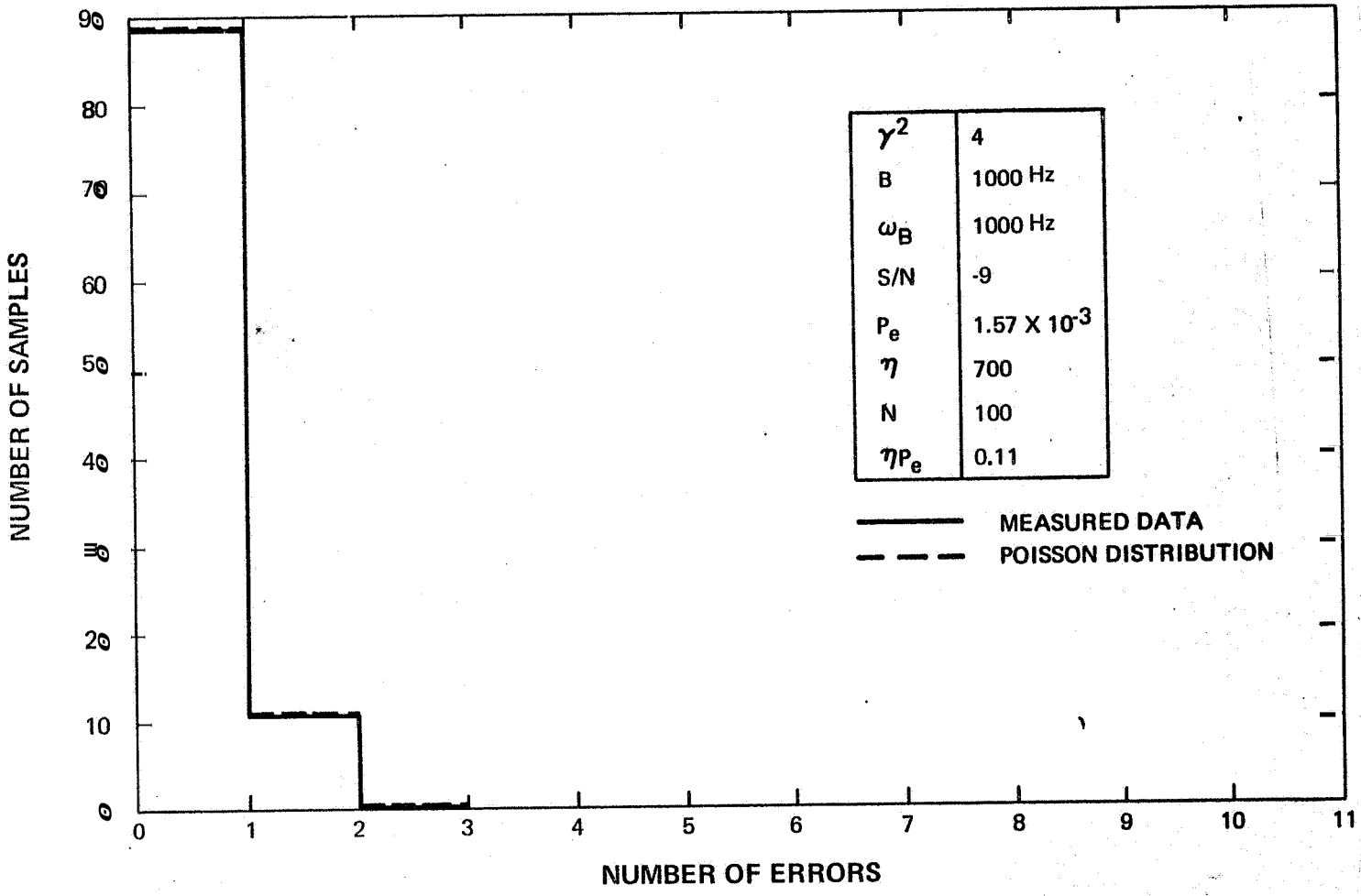

Figure V-6 Error Distribution for B = 1000 Hz, ω_B = 1000 Hz with $\gamma^2 = 4$

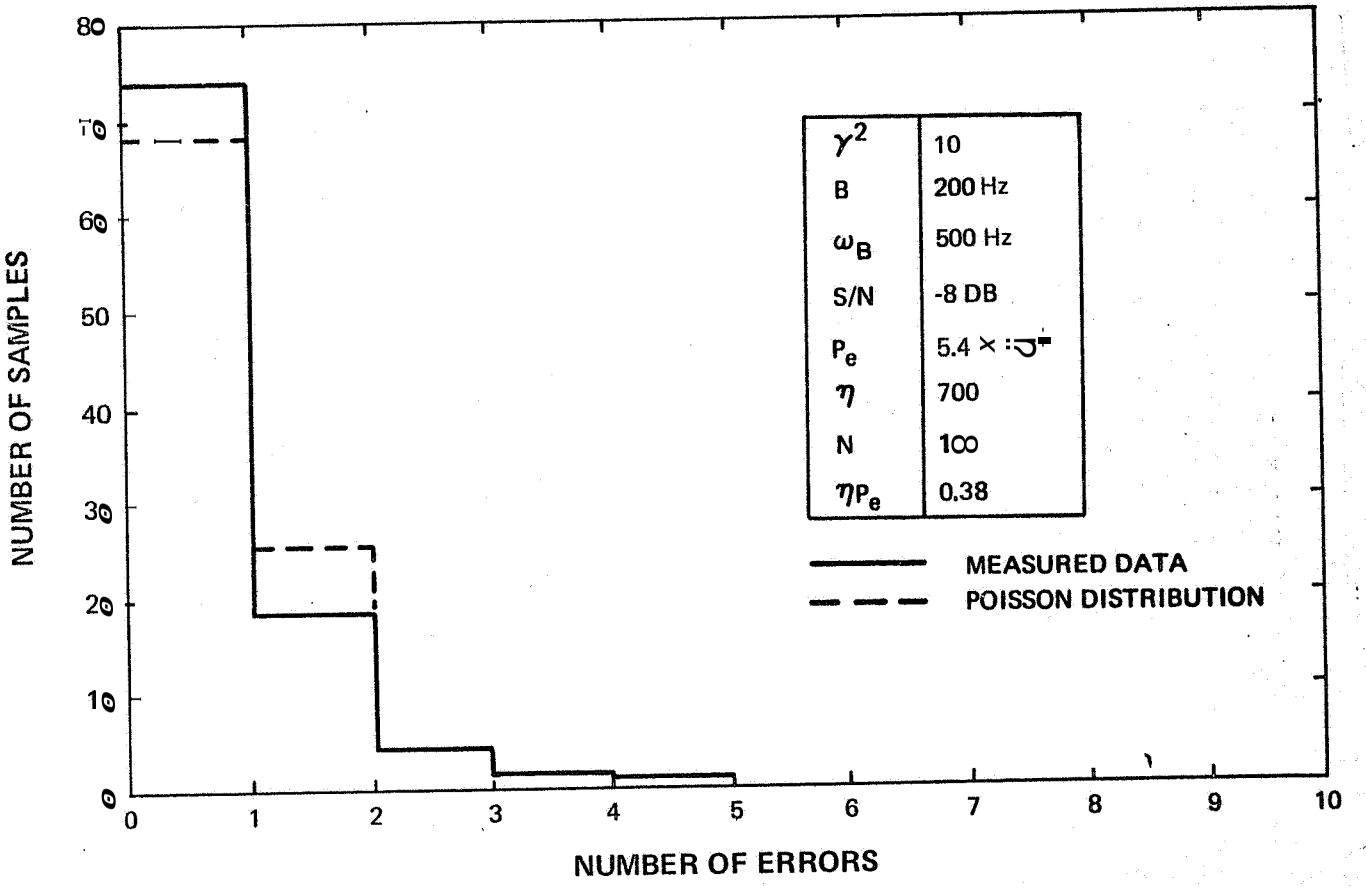

Figure V-7. Error Distribution for B = 200 Hz, ω_B = 500 Hz with $\gamma^2 = 10$

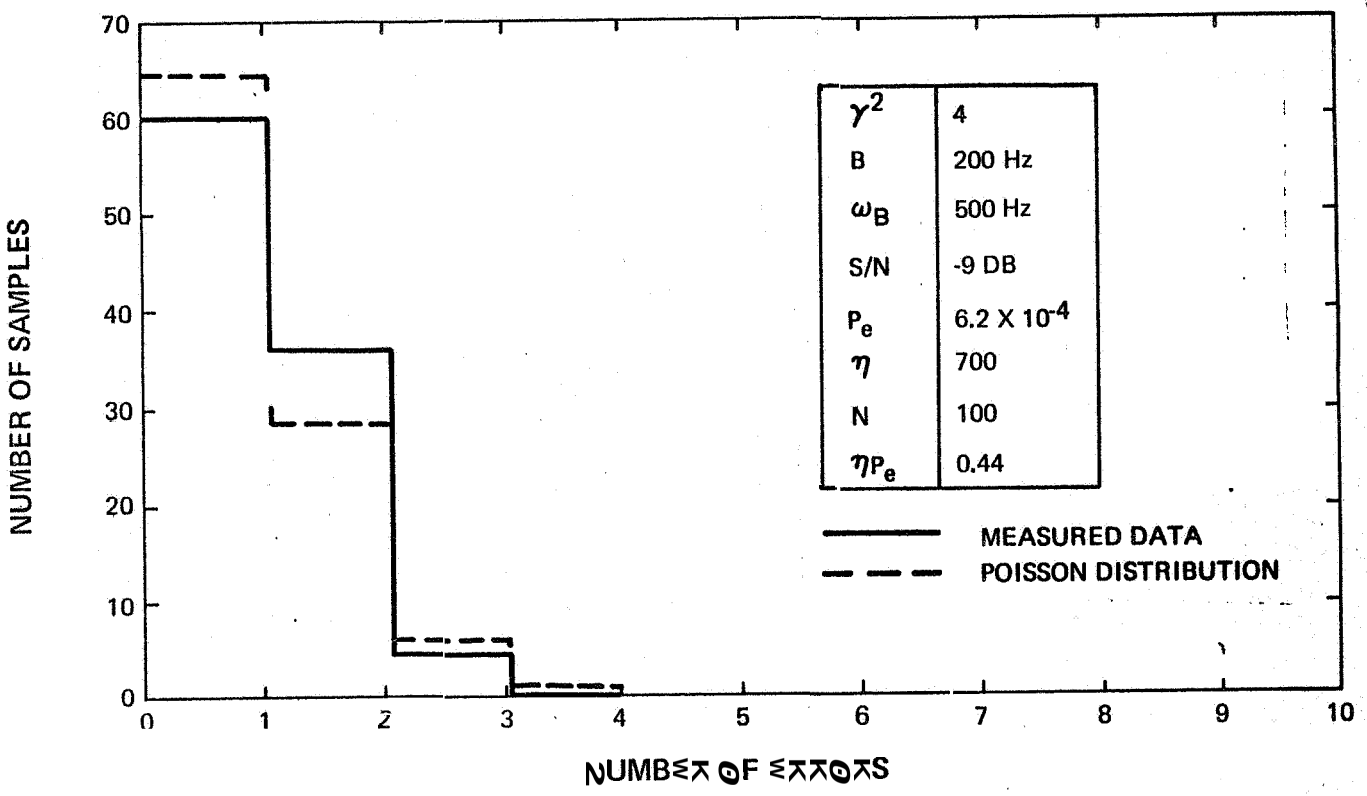

Figure V-8. Error Distribution for B = 200 Hz, ω_B = 500 Hz with $\gamma^2 = 4$

In each of these tests, the measured results compared favorably with the predicted values indicating that the multipath (under the stated conditions) did not cause a predisposition towards multiple errors. These results are not unexpected since as noted in Task 3 under the same conditions (Figures III-14, III-15, and III-16), multipath fading did not cause degradation of the link and actually provided improvement over the no-multipath case.

An additional series of tests was performed with fading bandwidths of 200 Hz with no doppler offset for $\gamma^2 = 10$, $\gamma^2 = 4$, and $\gamma^2 = 1$. Under these conditions in Task 3, there was pronounced degradation of the link due to the presence of multipath fading. If an effect on the error distribution is to occur, it would be more likely to occur under these conditions, since BT = 2, $\omega_B = 0$ and $\gamma^2 = 1$ are the expected worst cases. The results of these tests are shown in Figures V-9, V-10, and V-il. Even under these conditions, there is no experimental evidence of a higher incidence of multiple errors. This indicates that there is very little correlation of the fading effects from one bit period to the next. These results were surprising in view of the performance impact. The waveform photographs of Figure III-4, however, provided additional qualitative evidence to support the results. Observing the waveforms for the 200-Hz fading bandwidth over a bit period (10 milliseconds), there is no obvious correlation with the waveform in any other bit period.

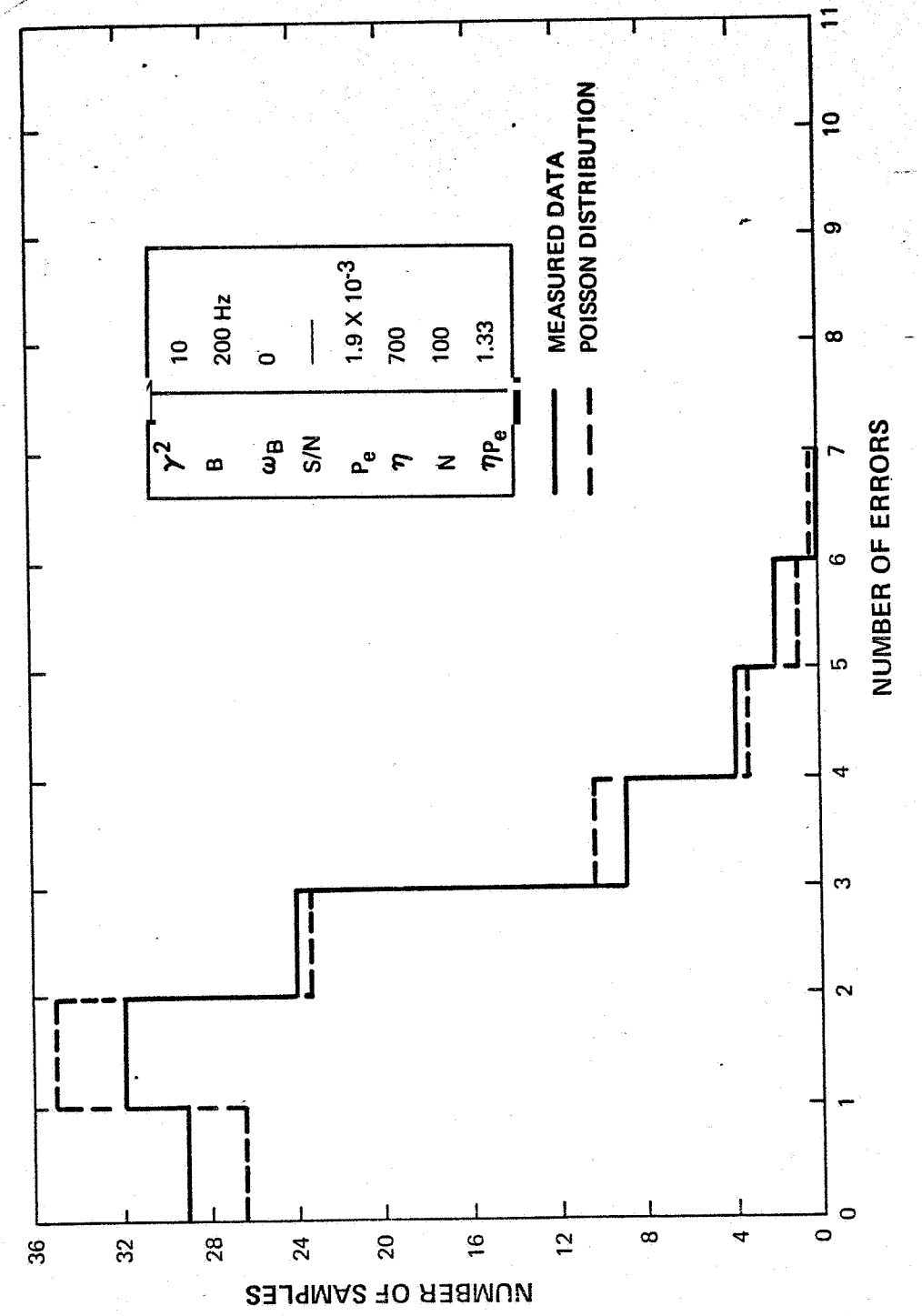

Figure V-9. Error Distribution for B = 200 Hz $\omega_B = 0$ with $\gamma^2 = 10$

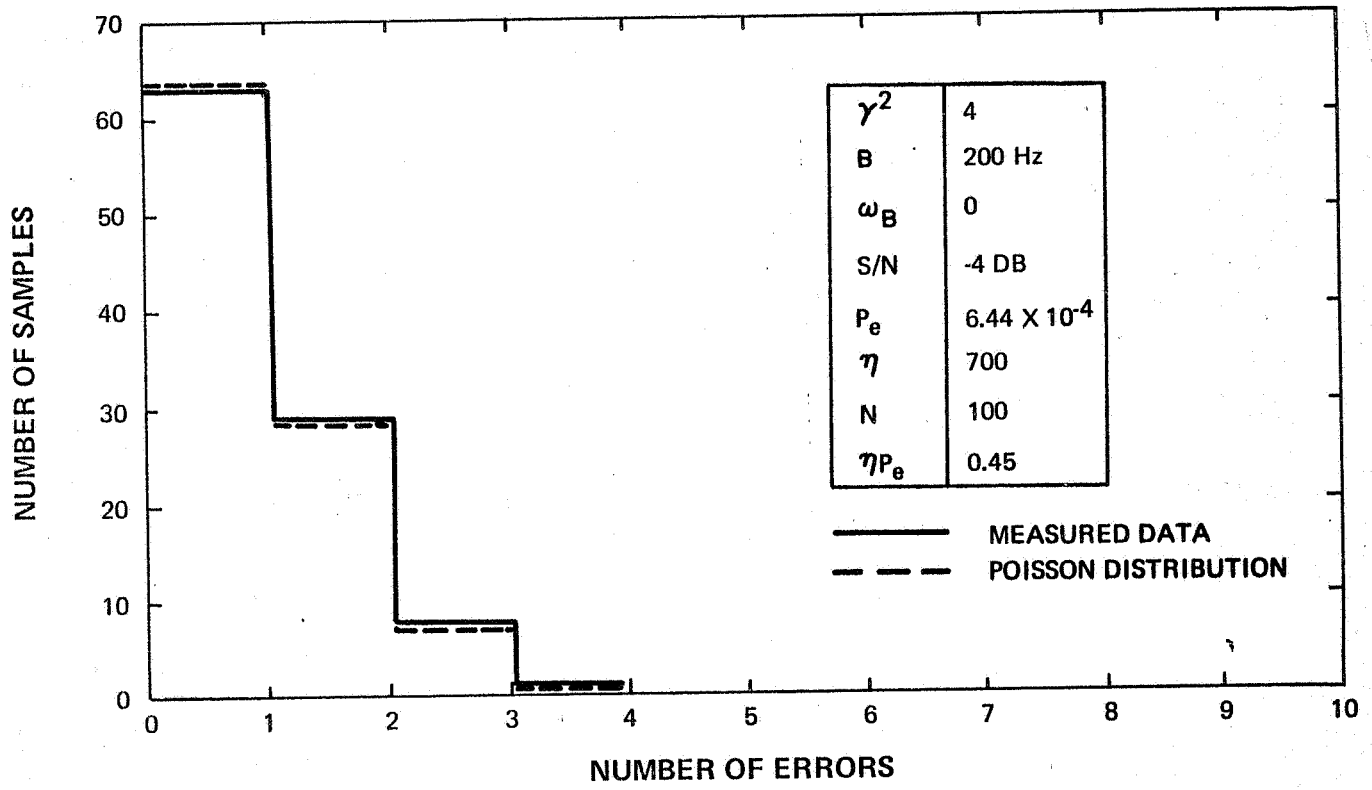

Figure V-10 E~~rror~~ Distribution for B = 200 Hz, $\omega_B = 0$ with $\gamma^2 = 4$

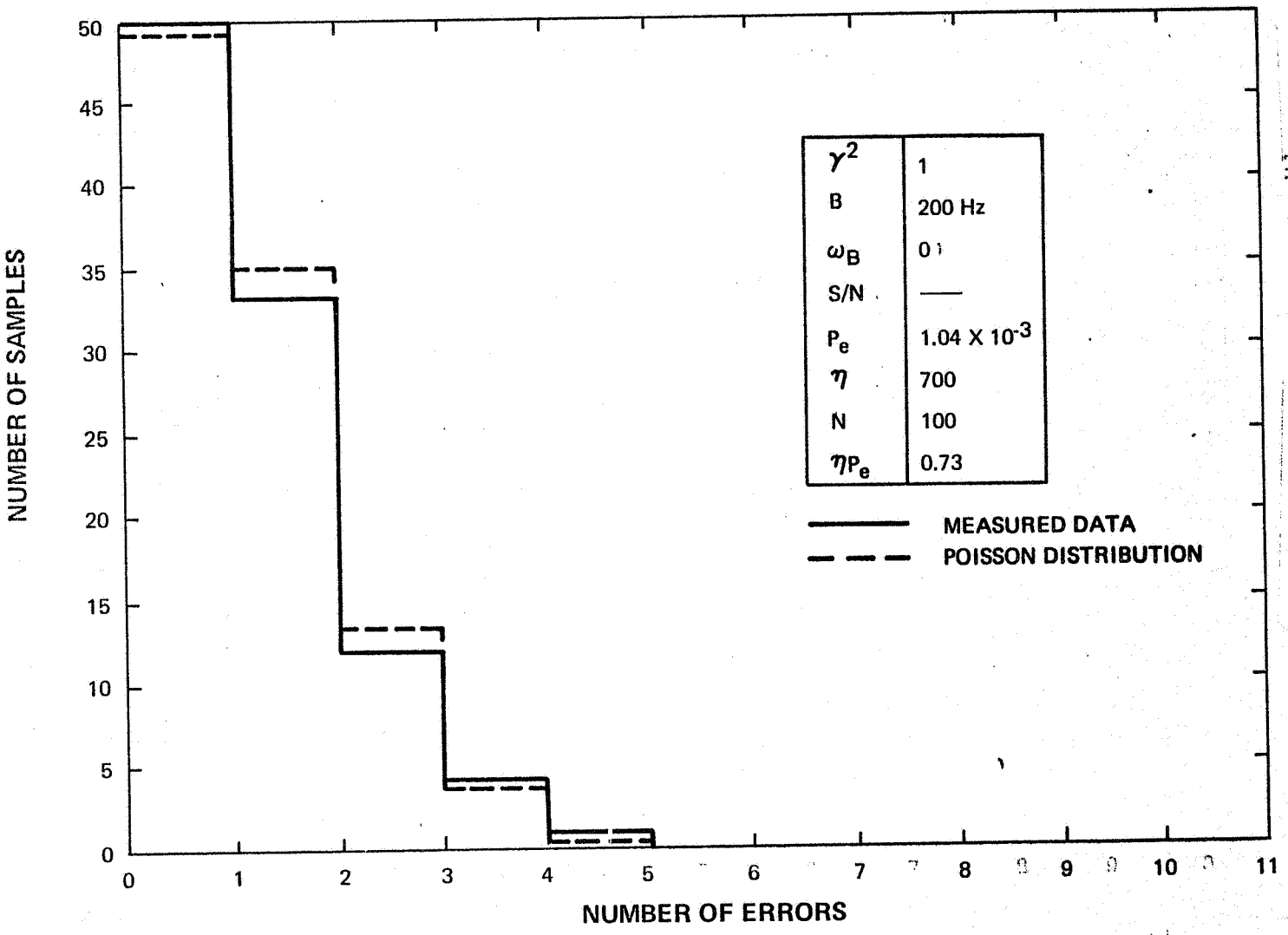

Figure 11. Error Distribution for B = 200 Hz, $\omega_B = 0$ with $\gamma^2 = 1$

D. CONCLUSIONS

In the case of very slow fading, it is known that deep fades occur which cause a large increase in the probability of error during that period of time. Therefore, in sampling the data, a higher number of errors would be expected during a fade, while conversely, a very small number of errors would be expetted during periods of reinforcement (which are equally likely as fades). The error distribution would then show a disproportionate tendancy toward extremes of small and large numbers of errors relative to that predicted by a mean error rate. The results of this experiment have shown that for BT products greater than two, this effect has not occurred. The errors are random and independent, with no tendency to cluster, and the average bit error rate is a valid measure of communications performance.